Control of Drosophila endocycles by E2F and CRL4(CDT2)

Zielke, N ; Kim, K J ; Tran, V ; Shibutani, S T ; Bravo, M J ; Nagarajan, S ; van Straaten, M ; Woods, B ; von Dassow, G ; Rottig, C ; Lehner, C F ; Grewal, S S ; Duronio, R J ; Edgar, B A

Abstract: Endocycles are variant cell cycles comprised of DNA synthesis (S)- and gap (G)-phases but lacking mitosis1,2. Such cycles facilitate post-mitotic growth in many invertebrate and plant cells, and are so ubiquitous that they may account for up to half the world's biomass3,4. DNA replication in endocycling Drosophila cells is triggered by cyclin E/cyclin dependent kinase 2 (CYCE/CDK2), but this kinase must be inactivated during each G-phase to allow the assembly of pre-Replication Complexes (preRCs) for the next S-phase5,6. How CYCE/CDK2 is periodically silenced to allow re-replication has not been established. Here, using genetic tests in parallel with computational modelling, we show that the endocycles of Drosophila are driven by a molecular oscillator in which the E2F1 transcription factor promotes CycE expression and S-phase initiation, S-phase then activates the CRL4CDT2 ubiquitin ligase, and this in turn mediates the destruction of E2F1 (ref. 7). We propose that it is the transient loss of E2F1 during S phases that creates the window of low Cdk activity required for preRC formation. In support of this model overexpressed E2F1 accelerated endocycling, whereas a stabilized variant of E2F1 blocked endocycling by deregulating target genes, including CycE, as well as Cdk1 and mitotic cyclins. Moreover, we find that altering cell growth by changing nutrition or target of rapamycin (TOR) signalling impacts E2F1 translation, thereby making endocycle progression growth-dependent. Many of the regulatory interactions essential to this novel cell cycle oscillator are conserved in animals and plants1,2,8, indicating that elements of this mechanism act in most growth-dependent cell cycles.

DOI: https://doi.org/10.1038/nature10579

Control of *Drosophila* endocycles by E2F and CRL4^{Cdt2}

Norman Zielke[1,2]*, Kerry J. Kim[3]*, Vuong Tran[2]*, Shusaku T. Shibutani[5], Maria-Jose Bravo[2], Sabarish Nagarajan[6], Monique van Straaten[1], Brigitte Woods[2], George von Dassow[3], Carmen Rottig[4], Christian F. Lehner[4], Savraj Grewal[6], Robert J. Duronio[5], and Bruce A. Edgar[1,2,7]

[1]German Cancer Research Center (DKFZ)-Zentrum für Molekulare Biologie der Universität Heidelberg (ZMBH) Alliance, Im Neuenheimer Feld 282, 69120 Heidelberg, Germany

[2]Fred Hutchinson Cancer Research Center, 1100 Fairview Avenue North, Seattle, WA 98109, USA

[3]Center for Cell Dynamics, Friday Harbor Labs, University of Washington, 620 University Rd., Friday Harbor, WA 98250, USA

[4]Zoologisches Institut, Universität Zürich, Winterthurerstr. 190, 8057 Zürich, Switzerland

[5]Department of Biology, University of North Carolina, Chapel Hill, NC 27599, USA

[6]Clark H. Smith Brain Tumor Center, Southern Alberta Cancer Research Institute, and Department of Biochemistry and Molecular Biology, University of Calgary, 3330 Hospital Drive, Calgary, Alberta, T2N 4N1, Canada

[7]Corresponding Author

*These authors contributed equally to this work.

(Nature 2009-05-04649B)

Endocycles are variant cell cycles comprised of DNA Synthesis (S)- and Gap (G)-phases but lacking mitosis[1,2]. Such cycles facilitate post-mitotic growth in many invertebrate and plant cells, and are so ubiquitous that they may account for up to half the world's biomass[3,4]. DNA replication in endocycling *Drosophila* cells is triggered by Cyclin E/Cyclin Dependent Kinase 2 (CycE/Cdk2), but this kinase must be inactivated during each G-phase to allow the assembly of pre-Replication Complexes (preRCs) for the next S-phase[5,6]. How CycE/Cdk2 is periodically silenced to allow re-replication has not been established. Here, using genetic tests in parallel with computational modeling, we show that *Drosophila's* endocycles are driven by a molecular oscillator in which the E2F1 transcription factor promotes *CycE* expression and S-phase initiation, S-phase then activates the CRL4^{Cdt2} ubiquitin ligase, and this in turn mediates the destruction of E2F1[7]. We propose that it is the transient loss of E2F1 during S-phases that creates the window of low Cdk activity required for preRC formation. In support of this model over-expressed E2F1 accelerated endocycling, whereas a stabilized variant of E2F1 blocked endocycling by de-regulating target genes including *CycE,* as well as *Cdk1* and mitotic *Cyclins*. Moreover, we find that altering cell growth by changing nutrition or TOR signaling impacts E2F1 translation, thereby making endocycle progression growth-dependent. Many of the regulatory interactions essential to this novel cell cycle oscillator are conserved in animals and plants[1,2,8], suggesting that elements of this mechanism act in most growth-dependent cell cycles.

S-phase control in proliferating animal cells depends upon the E3 ubiquitin ligase, $APC^{Fzy/Cdc20}$, which is activated by Cyclin/Cdk1 during mitosis. $APC^{Fzy/Cdc20}$ promotes the degradation of mitotic Cyclins, thereby extinguishing Cdk1 activity following mitosis, and it also promotes the degradation of Geminin (Gem), an inhibitor of the preRC component Cdt1. The combination of low Geminin and low Cyclin/Cdk1 activity during early G1 allows the assembly of preRCs containing origin recognition complex (ORC) proteins, Cdc6, Cdt1/Double-parked (Dup), and MCM2-7 onto replication origins, thus "licensing" the DNA for renewed replication[9]. *Drosophila's* endocycling cells do not express mitotic Cyclin/Cdk1 complexes or $APC^{Fzy/Cdc20}$ [10,11], and so this mechanism of S-phase regulation cannot apply to them. These endocycles do however employ CycE/Cdk2 to trigger S-phases[12,13] (Fig 1, 2), and they also require the G1-specific APC variant, $APC^{Fzr/Cdh1}$, which mediates cyclic degradation of cell cycle factors including Geminin and Orc1[10,14]. Importantly, while over-expressed CycE/Cdk2 is tolerated in mitotic cell cycles[15], it blocks endocycling (Fig 2, 3)[5,6]. This is likely due to CycE/Cdk2's ability to suppress $APC^{Fzr/Cdh1}$ and drive Geminin accumulation[10,14,16], though CycE may also inhibit preRC formation directly by phosphorylating preRC components. The importance of CycE oscillation for endocycling is underscored by the finding that Archipelago (Ago/Cdc4/Fbw7), which promotes CycE degradation as a component of an SCF ubiquitin ligase, is required for the progression of endocycles, but not mitotic cycles (Fig S1)[17]. Despite its importance the mechanism controlling CycE/Cdk2 periodicity in the endocycle has remained obscure for over a decade.

We addressed this problem in *Drosophila's* larval salivary glands, which undergo ~10 asynchronous endocycles from ~7-96 hours after egg deposition (h AED), reaching a final ploidy of ~1350C[18]. Studies in the fly ovary had suggested that the CycE/Cdk2 inhibitor *dacapo* (*dap*) might periodically silence Cdk2 during endocycling[19], but our analysis ruled this out for salivary glands (Fig S2)[10]. Hence we asked whether cyclic CycE/Cdk2 activity might be controlled transcriptionally. *CycE* transcription is regulated by the E2F1 transcription factor[20-22], the accumulation of which is periodic in mitotic *Drosophila* cells[7,23-25] because it is targeted for degradation during S-phase by the PCNA/replication fork-associated E3 ubiquitin ligase $CRL4^{Cdt2}$ [7]. In the salivary cells, *E2f1* mRNA was ubiquitous (Fig 1c) but E2F1 protein was cyclic, being virtually absent in S-phase nuclei (Fig 1d, 2a). Continuously over-expressed E2F1 proteins were also depleted from S-phase nuclei (Fig 2c, 3c), consistent with periodic degradation. This implied that E2F-dependent transcription might also oscillate. Indeed, the mRNAs encoding *CycE* and two other E2F targets, *RnrS* and *pcna* were periodic (Fig 1, 3, S15, see also[13]). These mRNAs accumulated when E2F1 was over-expressed (Fig 3a) and were reduced in mutants for *Dp*, E2F1's obligate dimerization partner (Fig S15). Thus periodic *CycE* expression is likely due to periodic activity of its regulator, E2F. CycE protein was also cyclic, being present during a bit of each Gap phase and much of each S-phase (Fig 1e)[13,26]. Based on these and other results[10] we determined that E2F1 accumulates during G-phases and is destroyed upon entry into S-phase, whereas its target CycE rises late in G-phases and persists through most of each S-phase.

These observations suggested that endocycles run using a molecular oscillator in which E2F1 promotes *CycE* transcription, and then CycE/Cdk2 triggers S-phase and the consequent destruction of E2F1 to reset the cycle (Fig 1g). To evaluate this hypothesis we built a computational model that translated known regulatory interactions into a system of delay differential equations describing the concentrations

of E2F1, RBF, CycE, Geminin, and Cdt1/Dup, and the activities of $APC^{Fzr/Cdh1}$ and $CRL4^{Cdt2}$ (Fig 1g, Supplementary Methods, Fig S4, S5). In this model, when CycE was low Gem was degraded by $APC^{Fzr/Cdh1}$, allowing preRC licensing through Cdt1/Dup. High CycE suppressed $APC^{Fzr/Cdh1}$ activity and allowed Gem accumulation, and also triggered phosphorylation of RBF, S-phase initiation, activation of $CRL4^{Cdt2}$ and the subsequent degradation of E2F1 and Cdt1/Dup. The model's behavior depended on unmeasured parameters representing biochemical kinetics (Table S1), but Monte-Carlo searches found numerous parameters sets that simulated actual endocycles (Fig 1h, i). The model robustly produced oscillations of its components despite quantitative parameter variation (Fig S6-9) and did not require exquisitely tuned kinetics to reproduce oscillations like those observed *in vivo* (Supplementary Discussion).

We tested the computational model by challenging it to reproduce the results of genetic experiments performed in parallel. The model reproduced nearly all observed mutant and gene over-expression phenotypes (Fig 2, S10). Notably, it predicted that increasing E2F1 should accelerate endocycling and lead to hyper-polyploidy, as subsequently observed experimentally (Fig 2, 3, S11). As predicted, we observed increased relative DNA amounts in $E2f1^{+/+}$ cells generated in an $E2f1^{+/-}$ background, and found that $E2f1^{7172}$ homozygous null mutant cells supported essentially no endocycling (Fig 2b, S13). Thus both loss- and gain-of-function experiments indicated that E2F1 is an essential dose-dependent regulator of endocycle progression.

An important prediction of the computational model was that periodic E2F1 destruction should be essential for endocycling. *Drosophila* E2F1 is targeted for proteolysis during S-phase via a conserved motif, the PIP box, which binds the replication fork-associated protein, PCNA, and mediates interaction with the $CRL4^{Cdt2}$ ubiquitin ligase[7]. Consistent with model predictions, a stabilized but active form of E2F1 lacking the PIP box $(GFP\text{-}E2F1^{PIP3A})$[7] blocked endocycle progression (Fig 2, 3, S11). Likewise RNAi against Cul4, a $CRL4^{Cdt2}$ component, arrested endocycling (Fig 2b, S11, S12). Levels of E2F1 in cells arrested by $GFP\text{-}E2F1^{PIP3A}$ were not higher than in control GFP-E2F1-expressing cells that cycled, suggesting that this arrest was due to inappropriately timed expression of E2F1 rather than its excessive accumulation (Fig 3h, S11). Hence S-phase dependent degradation of E2F1 is essential for endocycling.

One discrepancy between the data and our model was that whereas the model could not readily predict endocycling without E2F (Fig S10), *Dp* and *E2f1 E2f2* mutants support endocycling[21,22,26]. Our analysis showed that although Dp protein was barely detectable in *Dp* mutant glands (Fig S15) cells in these mutants nevertheless endocycled slowly and sustained periodic expression of *CycE* and *RnrS*, and Geminin oscillation (Fig 2b, S14, S15). One explanation for these apparently discrepant observations is that residual maternal E2F activity persists in these mutants. Consistent with this possibility we found that $GFP\text{-}E2F1^{PIP3A}$ was able to block endocycling in *Dp* mutants (Fig S16). Given this observation, the *Dp* mutant phenotype cannot be construed as confounding the model (see Supplementary Discussion).

We next asked how stabilized E2F1 arrests endocycling. Consistent with model predictions, cells arrested by $GFP\text{-}E2F1^{PIP3A}$ or Cul4-RNAi accumulated *CycE* and Geminin (Fig 3). In these arrested cells, however, Geminin accumulation occurred following rather than prior to arrest (Fig S12), indicating that it did not initiate the arrest. Interestingly, *gem* null mutant glands supported rather normal endocycles (Fig

S17), but arrest by Rca1[10,14], an APC$^{Fzr/Cdh1}$ inhibitor, was substantially rescued in the *gem* mutants (Fig 3e, S18). This demonstrates that the predominant function of APC$^{Fzr/Cdh1}$ in these endocycles is the degradation of Geminin. Importantly, *gem* mutant cell could be arrested by ectopic CycE[10,14] or E2F1^{PIP3A} (Fig 3e, S18, S19). We conclude that while Geminin accumulation might consolidate the arrest caused by excess E2F1, it is neither initiating nor essential for this arrest.

Further investigations revealed that Cyclin A, Cyclin B3 and Cdk1 accumulated in E2F1^{PIP3A}-arrested cells (Fig 3i, S20). These G2/M regulators are not normally expressed in endocycling cells[8,10]. Large inductions of the mRNAs encoding these factors were observed (Fig 3h), suggesting transcriptional de-repression. Consistent with this notion these factors were also induced in cells mutant for *E2f2*, *Drosophila's* repressor E2F (Fig 3i, j). This suggests that, as in mitotic cells[27], excess E2F1 may displace E2F2 and thereby de-repress its targets. In this context E2F2 appears to act as a selectivity factor that represses mitotic targets in endoreplicating cells. Given that Cdk1 is a potent suppressor of PreRCs that can arrest endocycle progression[6], its de-repression probably contributed to endocycle arrest by E2F1^{PIP3A}.

Altogether our results indicate that periodic E2F1 degradation is necessary for endocycling for three reasons: 1) it creates a window of low CycE/Cdk2 activity; 2) it promotes high APC$^{Fzr/Cdh1}$ activity and thereby suppresses Geminin accumulation; and 3) it allows E2F2 to maintain repression of Cdk1 and its Cyclins. Each of these conditions is required for preRC assembly and endocycle progression. This cell cycle mechanism (Fig 1g, S4) is fundamentally different from that used in mitotic cycles, wherein destruction of the M-phase Cyclins by APC$^{Cdc20/Fzy}$, rather than of E2F1 by the CRL4^{Cdt2}, throws the switch that allows preRC assembly[9]. Indeed it is noteworthy that the periodic degradation of E2F1 and depletion of CycE are not required for mitotic cell cycles in *Drosophila*[7,12]. CRL4^{Cdt2} is required for endocycling in plants[8], suggesting that this element of the endocycle oscillator is conserved.

Finally, we asked what factors control E2F production to regulate endocycle rates. Endocycle speed and number can be manipulated by altering cell growth through changes in dietary protein[28] or growth-regulatory genes including dMyc[1] and Insulin/PI3K/TOR signaling components[29]. Hence we starved larvae of protein to suppress insulin/TOR signaling, reduce protein synthesis, and block cell growth. Starvation arrested the salivary endocycles within 24h and strongly depleted E2F1 (Fig 4a,b). *E2f1* and *Dp* mRNA levels were not affected, but the E2F targets *CycE, pcna,* and *rnrS* were reduced (Fig 4c, not shown). To test whether this was responsible for starvation-induced endocycle arrest we overexpressed E2F1 in the salivary glands of starved animals. Although these glands failed to grow their nuclei incorporated BrdU and accrued ~7-fold more DNA than controls (Fig 4a). Over-expression of Rheb, which activates the *Target of Rapamycin (TOR)* kinase and increases ribosome biogenesis and cap-dependent translation, also restored cell growth, E2F1 protein, and endocycle progression in starved animals (Fig 4a). Thus E2F1 appears to act as a "growth sensor" that couples rates of endocycle progression to rates of cell growth. A likely mechanism for this, corroborated by modeling (Fig 4e, S8), involves increased translation of E2F1 in rapidly growing cells. Indeed, we found that the association of E2F1 mRNA with polyribosomes was greatly reduced in protein-starved animals (Fig 4d). Translational control of E2F is an attractive mechanism for coupling growth to G1/S progression not only in endocycling cells, but also in growth-dependent mitotic cells with extended G1 periods.

METHODS SUMMARY

Larvae were raised at 25^{o}C in uncrowded conditions, and salivary glands dissected and analyzed using standard *Drosophila* genetics and molecular biology methods. DNA quantifications were done using DAPI fluorescence from CCD images. Computational modeling used delay differential equations tracking the concentrations of mRNAs and proteins, and numerically solved in *Mathematica* 5.2 (Wolfram Research). Full descriptions of experimental and computational methods, genotypes, and reagents is included in the Online Methods section and Supplementary Information.

REFERENCES

1. Edgar, B.A. & Orr-Weaver, T.L. Endoreplication cell cycles: more for less. *Cell* **105**, 297-306 (2001).
2. Lilly, M.A. & Duronio, R.J. New insights into cell cycle control from the Drosophila endocycle. *Oncogene* **24**, 2765-75 (2005).
3. Sugimoto-Shirasu, K. & Roberts, K. "Big it up": endoreduplication and cell-size control in plants. *Curr Opin Plant Biol* **6**, 544-53 (2003).
4. Whitman, W.B., Coleman, D.C. & Wiebe, W.J. Prokaryotes: the unseen majority. *Proc Natl Acad Sci U S A* **95**, 6578-83 (1998).
5. Follette, P.J., Duronio, R.J. & O'Farrell, P.H. Fluctuations in cyclin E levels are required for multiple rounds of endocycle S phase in Drosophila. *Current Biology* **8**, 235-238 (1998).
6. Weiss, A., Herzig, A., Jacobs, H. & Lehner, C.F. Continuous Cyclin E expression inhibits progression through endoreduplication cycles in *Drosophila*. *Current Biology* **8**, 239-242 (1998).
7. Shibutani, S.T. et al. Intrinsic negative cell cycle regulation provided by PIP box- and Cul4Cdt2-mediated destruction of E2f1 during S phase. *Dev Cell* **15**, 890-900 (2008).
8. Roodbarkelari, F. et al. Cullin 4-ring finger-ligase plays a key role in the control of endoreplication cycles in Arabidopsis trichomes. *Proc Natl Acad Sci U S A* **107**, 15275-80.
9. Diffley, J.F. Regulation of early events in chromosome replication. *Curr Biol* **14**, R778-86 (2004).
10. Zielke, N., Querings, S., Rottig, C., Lehner, C. & Sprenger, F. The anaphase-promoting complex/cyclosome (APC/C) is required for rereplication control in endoreplication cycles. *Genes Dev* **22**, 1690-703 (2008).
11. Maqbool, S.B. et al. Dampened activity of E2F1-DP and Myb-MuvB transcription factors in Drosophila endocycling cells. *J Cell Sci* **123**, 4095-106 (2010).
12. Knoblich, J.A. et al. Cyclin E controls S-phase progression and its down-regulation during *Drosophila* embryogenesis is required for the arrest of cell proliferation. *Cell* **77**, 107-120 (1994).
13. Lilly, M.A. & Spradling, A.C. The Drosophila endocycle is controlled by Cyclin E and lacks a checkpoint ensuring S-phase completion. *Genes & Development* **10**, 2514-2526 (1996).
14. Narbonne-Reveau, K. et al. APC/CFzr/Cdh1 promotes cell cycle progression during the Drosophila endocycle. *Development* **135**, 1451-61 (2008).
15. Neufeld, T.P., de la Cruz, A.F., Johnston, L.A. & Edgar, B.A. Coordination of growth and cell division in the Drosophila wing. *Cell* **93**, 1183-93 (1998).
16. Sigrist, S.J. & Lehner, C.F. Drosophila fizzy-related down-regulates mitotic cyclins and is required for cell proliferation arrest and entry into endocycles. *Cell* **90**, 671-81 (1997).

17. Shcherbata, H.R., Althauser, C., Findley, S.D. & Ruohola-Baker, H. The mitotic-to-endocycle switch in Drosophila follicle cells is executed by Notch-dependent regulation of G1/S, G2/M and M/G1 cell-cycle transitions. *Development* **131**, 3169-81 (2004).
18. Hammond, M.P. & Laird, C.D. Control of DNA replication and spatial distribution of defined DNA sequences in salivary gland cells of *Drosophila melanogaster*. *Chromosoma* **91**, 279-86 (1985).
19. Hong, A. et al. The cyclin-dependent kinase inhibitor Dacapo promotes replication licensing during Drosophila endocycles. *Embo J* **26**, 2071-82 (2007).
20. Duronio, R.J. & O'Farrell, P.H. Developmental control of the G_1 to S transition in *Drosophila*: cyclin E is a limiting downstream target of E2F. *Genes and Development* **9**, 1456-1468 (1995).
21. Royzman, I., Whittaker, A.J. & Orr-Weaver, T.L. Mutations in *Drosophila DP* and *E2F* distinguish G_1-S progression from an associated transcriptional program. *Genes and Development* **11**, 1999-2011 (1997).
22. Duronio, R.J., Bonnette, P.C. & O'Farrell, P.H. Mutations of the Drosophila dDP, dE2F, and cyclin E genes reveal distinct roles for the E2F-DP transcription factor and cyclin E during the S-phase transition. *Molecular and Cellular Biology* **18**, 141-151 (1998).
23. Asano, M., Nevins, J.R. & Wharton, R.P. Ectopic E2F expression induces S-phase and apoptosis in *Drosophila* imaginal discs. *Genes and Development* **10**, 1422-1432 (1996).
24. Reis, T. & Edgar, B.A. Negative regulation of dE2F1 by cyclin-dependent kinases controls cell cycle timing. *Cell* **117**, 253-64 (2004).
25. Heriche, J.K., Ang, D., Bier, E. & O'Farrell, P.H. Involvement of an SCFSlmb complex in timely elimination of E2F upon initiation of DNA replication in Drosophila. *BMC Genet* **4**, 9 (2003).
26. Weng, L., Zhu, C., Xu, J. & Du, W. Critical role of active repression by E2F and Rb proteins in endoreplication during Drosophila development. *Embo J* **22**, 3865-75 (2003).
27. Frolov, M.V. et al. Functional antagonism between E2F family members. *Genes & Development* **15**, 2146-60 (2001).
28. Britton, J.S. & Edgar, B.A. Environmental control of the cell cycle in Drosophila: nutrition activates mitotic and endoreplicative cells by distinct mechanisms. *Development* **125**, 2149-58 (1998).
29. Britton, J.S., Lockwood, W.K., Li, L., Cohen, S.M. & Edgar, B.A. Drosophila's insulin/PI3-kinase pathway coordinates cellular metabolism with nutritional conditions. *Dev Cell* **2**, 239-49 (2002).

SUPPLEMENTARY INFORMATION

ACKNOWLEDGEMENTS

Supported by NIH GM51186 to B.A.E., DKFZ, a DAAD fellowship to N.Z., NIGMS 5 P50 GM66050 and NSF MCB0090835 to G.v.D. and K.J.K, DFG LE987/5-1 to C.F.L., CIHR MOP-86622 to S.G., and NIH GM57859 to R.J.D. We thank Yan Liu for help with statistics.

AUTHOR CONTRIBUTIONS

The E2F1-based oscillator was conceived by B.A.E.. N.Z. developed the framework for licensing control and E2F2-mediated repression of mitotic genes. K.J.K. did most of the computational modeling, which was initiated by G.v.D.. Initial experiments were done by V.T., who, with help from B.W. and K.J.K., contributed Fig 1d-f, 2a-b, 4a-b

and S13. N.Z. carried out much of the later experimental work with help from M.v.S, and contributed Fig 2b-c, 3c-j, 4c, S1, S3, S11, S12 and S14-20. S.T.S and R.J.D. contributed the GFP-E2F1^{PIP3A} transgenics and controls. M.J.B. contributed Fig 1A-C, 3A-B and S15 G-H. S.N. and S.G. contributed Fig 4D. C.R. and C.F.L. contributed Fig S2 and the *cdk2*$^{-/-}$ data in Fig 2B. B.A.E. directed the project and wrote the manuscript.

AUTHOR INFORMATION

FIGURE LEGENDS

Figure 1. Wildtype salivary gland endocycles.
a-c) *In situ* hybridization of WT 72h AED glands to the indicated mRNAs. **d-f)** WT salivary glands at 72h AED double-labeled for: **d)** E2F1 (green) and BrdU (red); **e)** CycE (red) and BrdU (green); **f)** CycE (red) and E2F1 (green). Graphs show nuclear concentrations measured from micrographs of 2-3 glands, in which each dot represents one nucleus. Shaded region (blue) shows trajectory of E2F1/CycE oscillations with an arrow indicating the expected temporal progression. **g)** Simplified schematic of the computational model. See Fig S4. **h)** Time plot for WT predicted by the model. **i)** Nuclear concentrations predicted by the model; arrow represents temporal progression.

Figure 2. Genetic tests of the endocycle mechanism.
a) Salivary glands (centered) and associated fat body (above or below; FB) from 72h AED larvae expressing the indicated genes under *ptc-Gal4/UAS* control. *ptc-Gal4* expresses in salivary glands but not in fat body. Left column shows DNA (blue) and BrdU (red) incorporated from 71-72h AED. Middle column shows E2F1 (green). Right column shows E2F1 and BrdU. All images had identical exposures and magnifications. Graphs (right) show simulated time plots of E2F1 (green) CycE (red) protein levels and CRL4^{Cdt2} (Cul4-E3) activity (blue) for each genotype. See Table S1 for parameters. **b)** Nuclear DNA values from 96h AED glands. For each genotype about 40 nuclei from 6-20 salivary glands were analyzed. Error bars represent standard deviations. *ptc-Gal4* drove expression of the UAS-linked transgenes indicated with a "+". *Dp*$^{-/-}$: *Dp*^{a2}*/Df(2R)Exel7124* mutant. *E2f1*$^{-/-}$ *: E2f1*^{7172} mutant cells generated by mitotic recombination. *cdk2*$^{-/-}$ mutant glands were generated as described in methods. **c)** Salivary glands expressing wild-type GFP-E2F1 (above) or GFP-E2F1^{PIP3A} (below). Layout as in **a**.

Figure 3. Endocycle arrest by stabilized E2F1.
a-d) Expression of WT GFP-E2F1 with *ptc-Gal4* promoted endocycling with cyclic *cycE* (**a**) and Gem (**c**), whereas GFP-E2F^{PIP3A} caused endocycle arrest with uniform *cycE* (**b**) and Gem (**d**) expression. **e)** C-values per nucleus for the indicated genotypes and timepoints. For each genotype about 40 nuclei from 10-20 salivary glands were analyzed. Error bars represent standard deviations. **f-g)** CycA expression in WT (**f**) and glands expressing WT GFP-E2F1 (**f**) or GFP-E2F^{PIP3A} (**g**). Arrowhead (**f**) indicates diploid imaginal ring cells. **h)** qRT-PCR measurements of the indicated mRNAs, from 72h AED salivary glands expressing GFP-E2F1 (green) or GFP-E2F1^{PIP3A} (red). **i)** CycA and Cdk1 accumulation in *E2f2* mutant cells, generated by MARCM mitotic recombination. GFP in **i** marks mutant cells (outlined). Cdk1 in **i'''** was detected using anti-PSTAIRE antibody. **j)** qRT-PCR measurements of the indicated mRNAs, from *E2f2* mutant glands at the indicated timepoints. Log10(Ratio)s

for **h** and **j** are relative to WT controls. Error bars represent standard deviations derived from 3-4 biological replicates.

Figure 4. E2F1 is a growth sensor.
a) Salivary glands labeled for DNA (blue), E2F1 (green), and incorporated BrdU (red). Fed Control (WT) was labeled with BrdU at 48h and fixed at 49h. **"**Starved" animals were transferred to protein-free media at 48h AED, labeled with BrdU at 96h, and fixed at 97h AED. *ptc-Gal4* drove expression of *UAS-E2F1/DP* or *UAS-Rheb* in the lower two panels. Chromatin (C) values are average nuclear DNA values from 10 glands measured at 120h AED. **b)** Immunoblot of salivary glands as in **a**, with quantitation, normalized to tubulin, below. **c)** mRNA levels from starved and fed control glands, measured by qRT-PCR. **d)** mRNA levels from 3d protein-starved (black) or fed control (red) whole larvae, quantified from polysome gradient fractions by qRT-PCR. X axis indicates gradient fraction number. **e)** Computational simulation of starvation by reducing total protein synthesis (tn). In the "20% tn +E2F1" graph, translation of E2F1 was 100% of normal but translation of all other proteins was reduced to 20%. Graphed values (**b, c**) include standard deviations calculated from 3 independent biological samples.

METHODS

Genetics

To express genes in salivary glands *ptc-Gal4, 43B-Gal4* or *hey-Gal4* females were crossed to males carrying *UAS* transgenes. *E2f1*^{7172}*/ E2f1*^{7172} mutant salivary gland cells were generated by heat shocking *hs-Flp; FRT82B E2f1*^{7172}*/FRT82B ub-GPF-nls* embryos to 37^{o}C from 2-4h AED. *Cdk2* mutant glands were generated using the genotype: *F4-Gal4 UAS-GFP/+; Cdk2FRT Cdk2*^{3}*/Cdk2*^{2} or *F4-Gal4 UAS-GFP/UAS-Flp; Cdk2FRT Cdk2*^{3}*/Cdk2*^{2}*,* where *Cdk2FRT* is a transgene encoding an Flp-excisable Cdk2.

Mutants:
w; FRT80B, *ago*^{1}/TM6B[30]
y,w, hs-FLP$^{1.22}$*;* FRT80B P[mini-w], P[*ubi*-GFP]/TM6B
dap^{4}/CyO*, act*-GFP[31]
dap^{g36}/CyO*, act*-GFP[32]
w; Dp^{a1} /CyO, *act*-GFP[21]
w; Dp^{a2} /CyO, *act*-GFP[21]
w; FRT42D, *Dp*^{a3} /CyO, *act*-GFP[21,33]
w; Df(2R)Exel7124 /CyO(*act*-GFP) (Bloomington *Drosophila* Stock Center #7872)
w; FRT80B, *e2f1*^{7172}/TM6B (*e2f1*^{7172} is described in [34])
w; *e2f2*^{76Q1}, *cn*, *bw*/CyO, *act*-GFP[27]
w; FRT40A, *e2f2*^{C03344}, *dp*^{ov}/CyO, *act*-GFP (Gift from Maxim Frolov, University of Illinois, Chicago/USA)
w; *geminin*$^{l(2)k14019}$,*c*, *px*, *sp*/CyO, *act*-GFP[35]
w; *geminin*$^{l(2)k02302}$,*c*, *px*, *sp*/CyO, *act*-GFP[35]
w; DF(2R)ST1, Adh^{n5}, *pr*^{1}, *cn**/ CyO, *act*-GFP[35]

For mutants, we used the strongest alleles available, which in most cases are null alleles. Details on mutant lesions can be found in the cited papers and FlyBase (http://flybase.org/).

Transgenes:
ptc-Gal4[36]

43B-Gal4[5]
hey-Gal4, Pin/CyO (Gift from Amir Orian, Rappaport Institute, Israel)
UASt-Cul4-RNAi (VDRC #44829)
UASt-CycE[31]
UASt-CycE-RNAi (Nig-Fly #3938R-3)
UASt-Dap[31]
UASp-GFP-E2F1[7]
UASp-GFP-E2F1-PIP3A[7]
UASt-E2F1[15]
UASt-Rbf1[37]
UASt-Rheb[38]
UASt-HA-Rca1[39]

Starvation

At 48h or 72h AED larvae were washed with PBS and transferred to PBS+20% sucrose at 25^{o}C, and maintained on this media until 96h or 120h AED, respectively.

DNA quantification

DNA content in nuclei or whole salivary glands was quantified by DAPI fluorescence. Larvae were raised at 25^{o}C to 96h AED, and fixed glands were dissected and stained, using an internal control *(ptc-Gal4 UAS-GFPnls)* for each sample. Samples were imaged at 10x with a CCD camera (Spot RT or Roper HQ2). Average cytoplasmic intensity was subtracted, and the integrated DAPI intensity was used to measure DNA content for whole glands (Fig 2) or nuclei (Fig 3). All salivary glands had ~the same number of cells (<10% variability). Controls were set to 1350C according to[18].

Quantification of nuclear concentrations

Nuclear BrdU, Cyclin E, E2F1, and GFP-E2F1 concentrations as shown in Fig 1(D-F), S3, and S11 were measured from samples stained with DAPI and the indicated antibodies and imaged by confocal microscopy at 20X. We took image stacks (interval size = 0.65µm; optimal overlap under our conditions) with optimized imaging conditions such that the deviation from linearity was <10%. To measure average nuclear concentrations of E2F1 and CycE, we used ImageJ (NIH) and custom software that searched for nuclei by finding ellipsoidal regions that stained brightly for DNA and had the approximate diameter of a nucleus. About half of all nuclei visually overlapped with their neighbors and were not analyzed. To reproducibly set the boundaries for each nucleus, we restricted our analysis to optical sections in which the average nuclear DNA staining was >90% maximal (typically 2-5 sections). Mean intensity in these regions was measured in other channels to determine nuclear concentrations.

BrdU labeling

Embryos were collected on grape-juice/agar plates for 2h and transferred to regular fly-food 24h after egg deposition. At the indicated time points salivary glands were dissected in *Drosophila* Ringer's Solution and incubated for 1h at room temperature with 100µg/ml BrdU in Ringer's Solution. Afterwards, the samples were fixed for 30min in 4% Paraformaldehyde/PBS and subsequently treated for 30min with 2N HCl. BrdU incorporation was detected with a mouse anti-BrdU antibody (Becton Dickinson) diluted 1:20 in 4% NGS/PBS/0.3% Triton-X100 and goat anti-mouse-Alexa Fluor-568 (Invitrogen) as secondary antibody diluted 1:2000 in 4% NGS/PBS/0.3% Triton-X100.

EdU labeling

EdU incorporation was performed analogous to the procedure for BrdU labeling using the Click-It EdU Alexa Fluor-555 imaging kit from Invitrogen.

In situ hybridization

Probes for in situ hybridization were generated with the DIG RNA labeling system (Roche). For in vitro transcription with T7/T3 RNA polymerase the following plasmids were used as template: pT7T3-19U-CycE[40]; pBLu(2)SKM-RnrS[41]; pBluSKP-E2F1[42]. Salivary glands were dissected from larvae staged to the indicated time points. Small batches of about 30 larvae were fixed overnight in 8% formaldehyde/PBS, pooled in scintillation vials and stored until usage in ethanol at -80˚C. The hybridization procedure was performed according to the protocol developed by the Bier-Lab[43]. For detection samples were probed with the following antibodies: sheep-anti-DIG-AP (1:500, Roche) or mouse anti-DIG-HRP (1:500, Abcam). BCIP/NBT was used as substrate for the AP reaction according to Tautz & Pfeifle[44], while the TSA Alexa Fluor-568 Detection Kit (Invitrogen) was used in combination with HRP.

qRT-PCR

At the indicated time points about 50 salivary glands per genotype were dissected in *Drosophila* Ringer's Solution and immediately transferred to the lysis-buffer supplied with the RNAeasy mini kit (Qiagen). Samples were stored at -80˚C and then processed with the RNAeasy mini kit (Qiagen) according the manufacturers instructions including the optional on-column DNAseI digestion. 100ng of total RNA were used for cDNA synthesis with the Quantitect Reverse Transcription Kit (Qiagen) or the iScript cDNA synthesis kit (Bio-Rad). qRT-PCR data shown in Figure 3 I-K was acquired on a Light Cycler 480 (Roche) using the indicated UPL assays (Roche) and Light Cycler 480 Probes Master (Roche). Relative expression data presented in Figure 4C was acquired on an iQ5 Instrument (Biorad) using QuantiTect Primer Assays (Qiagen) and the iScript one-step RT-PCR SYBR green kit (Bio-Rad). To ensure statistical significance qRT-PCR was performed in quadruplicates from 3-4 independent samples. Relative expression to GAPDH1 and Actin5c was determined with the ΔΔCT method:

$$\Delta CT = CT_{\text{gene of interest}} - CT_{\text{endogenous control}}$$

$$\Delta\Delta CT = \Delta CT_{\text{sample}} - \Delta CT_{\text{calibrator}}$$

$$\text{relative quantity} = 2^{-\Delta\Delta CT}$$

Polysome profiling

Whole larvae were lysed in ice-cold polysome lysis buffer (25mM Tris pH6.8, 10mM $MgCl_2$, 25mM NaCl, 1% Triton-X 100, 0.5% Sodium Deoxycholate, 0.5uM DTT 1ug/ml Cycloheximide, 10ug/ml Heparin, Protease Inhibitor Cocktail (Complete mini, Roche), 2.5 uM PMSF, 5mM Sodium Fluoride, 1mM Sodiumorthovanadate, RNase inhibitor (Ribolock, -Fermentas) using a Dounce Homogenizer. Lysates were then cleared by centrifugation (15,000 rpm, 15 mins, 4C). Equal optical density units (260nM) of cleared lysates were then layered on 15-45% sucrose gradient (prepared in polysome lysis buffer) and centrifuged (37,000 rpm, 2.5 hrs, 4C) in an SW41 Beckman rotor. The gradients were then fractionated using a Brandel BR188 Density Gradient fractionator with continuous OD (254nm) reading and collected into twelve equal fractions. The RNA from each fraction was extracted with Trizol reagent and reversed transcribed using Superscript II (Invitrogen) according to the manufacturers instructions. Quantitative real-time PCR was then performed as described in [45] using a MyIQ PCR machine (BioRad).

REFERENCES (Continued)

30. Moberg, K.H., Mukherjee, A., Veraksa, A., Artavanis-Tsakonas, S. & Hariharan, I.K. The Drosophila F box protein archipelago regulates dMyc protein levels in vivo. *Curr Biol* **14**, 965-74 (2004).
31. Lane, M.E. et al. Dacapo, a cyclin-dependent kinase inhibitor, stops cell proliferation during *Drosophila* development. *Cell* **87**, 1225-1235 (1996).
32. Lane, M.E. et al. A screen for modifiers of cyclin E function in Drosophila melanogaster identifies Cdk2 mutations, revealing the insignificance of putative phosphorylation sites in Cdk2. *Genetics* **155**, 233-44 (2000).
33. Frolov, M.V., Moon, N.S. & Dyson, N.J. dDP is needed for normal cell proliferation. *Mol Cell Biol* **25**, 3027-39 (2005).
34. Duronio, R.J., O'Farrell, P.H., Xie, J.-E., Brook, A. & Dyson, N. The transcription factor E2F is required for S phase during *Drosophila* embryogenesis. *Genes and Development* **9**, 1445-1455 (1995).
35. Quinn, L.M., Herr, A., McGarry, T.J. & Richardson, H. The Drosophila Geminin homolog: roles for Geminin in limiting DNA replication, in anaphase and in neurogenesis. *Genes Dev* **15**, 2741-54 (2001).
36. Speicher, S.A., Thomas, U., Hinz, U. & Knust, E. The *Serrate* locus of *Drosophila* and its role in morphogenesis of the wing imaginal discs: control of cell proliferation. *Development* **120**, 535-544 (1994).
37. Xin, S., Weng, L., Xu, J. & Du, W. The role of RBF in developmentally regulated cell proliferation in the eye disc and in Cyclin D/Cdk4 induced cellular growth. *Development* **129**, 1345-56 (2002).
38. Saucedo, L.J. et al. Rheb promotes cell growth as a component of the insulin/TOR signalling network. *Nat Cell Biol* **5**, 566-71 (2003).
39. Grosskortenhaus, R. & Sprenger, F. Rca1 inhibits APC-Cdh1(Fzr) and is required to prevent cyclin degradation in G2. *Dev Cell* **2**, 29-40 (2002).
40. Richardson, H.E., O'Keefe, L.V., Reed, S.I. & Saint, R. A *Drosophila* G1-specific cyclin E homolog exhibits different modes of expression during embryogenesis. *Development* **119**, 673-690 (1993).
41. Duronio, R.J. & O'Farrell, P. Developmental control of a G1-S transcriptional program in *Drosophila*. *Development* **120**, 1503-1515 (1994).
42. Dynlacht, B.D., Brook, A., Dembski, M., Yenush, L. & Dyson, N. DNA-binding and trans-activation properties of *Drosophila* E2F and DP proteins. *Proceedings of the National Academy of Sciences USA* **91**, 6359-6363 (1994).
43. Kosman, D. et al. Multiplex detection of RNA expression in Drosophila embryos. *Science* **305**, 846 (2004).
44. Tautz, D. & Pfeifle, C. A non-radioactive in situ hybridization method for the localization of specific RNAs in *Drosophila* embryos reveals translational control of the segmentation gene hunchback. *Chromosoma* **98**, 81-85 (1989).
45. Van Gilst, M.R., Hadjivassiliou, H. & Yamamoto, K.R. A Caenorhabditis elegans nutrient response system partially dependent on nuclear receptor NHR-49. *Proc Natl Acad Sci U S A* **102**, 13496-501 (2005).

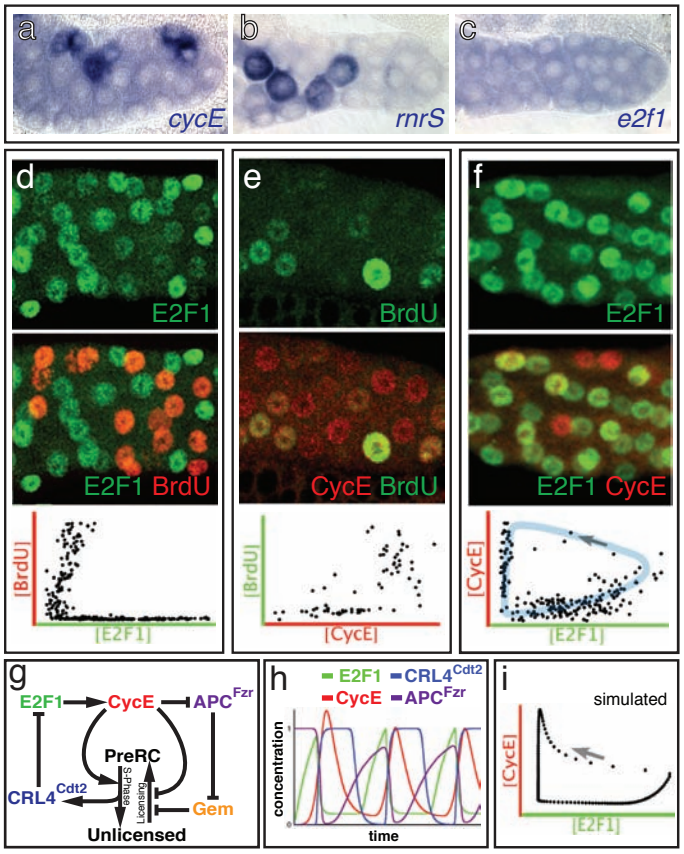
a
cycE
b
rnrS
c
e2f1
d
E2F1
E2F1 BrdU
[BrdU]
[E2F1]
e
BrdU
CycE BrdU
[BrdU]
[CycE]
f
E2F1
E2F1 CycE
[CycE]
[E2F1]
g
E2F1
CycE
APC^Fzr
PreRC
CRL4^Cdt2
S-Phase
Licensing
Gem
Unlicensed
h
E2F1
CRL4^Cdt2
CycE
APC^Fzr
concentration
time
i
simulated
[CycE]
[E2F1]

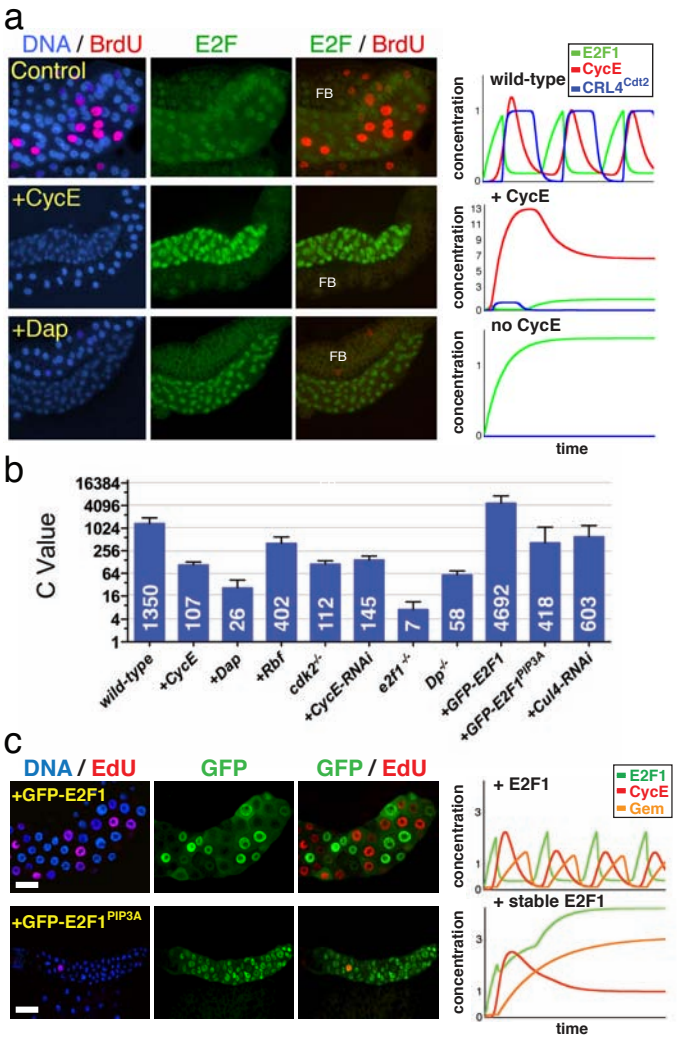
a
DNA / BrdU
E2F
E2F / BrdU
Control
+CycE
+Dap
FB
FB
FB
wild-type
E2F1
CycE
CRL4Cdt2
+ CycE
no CycE
concentration
time
b
C Value
16384
4096
1024
256
64
16
4
1
1350
107
26
402
112
145
7
58
4692
418
603
wild-type
+CycE
+Dap
+Rbf
cdk2-/-
+CycE-RNAi
e2f1-/-
Dp-/-
+GFP-E2F1
+GFP-E2F1PIP3A
+Cul4-RNAi
c
DNA / EdU
GFP
GFP / EdU
+GFP-E2F1
+GFP-E2F1PIP3A
+ E2F1
+ stable E2F1
E2F1
CycE
Gem
concentration
time

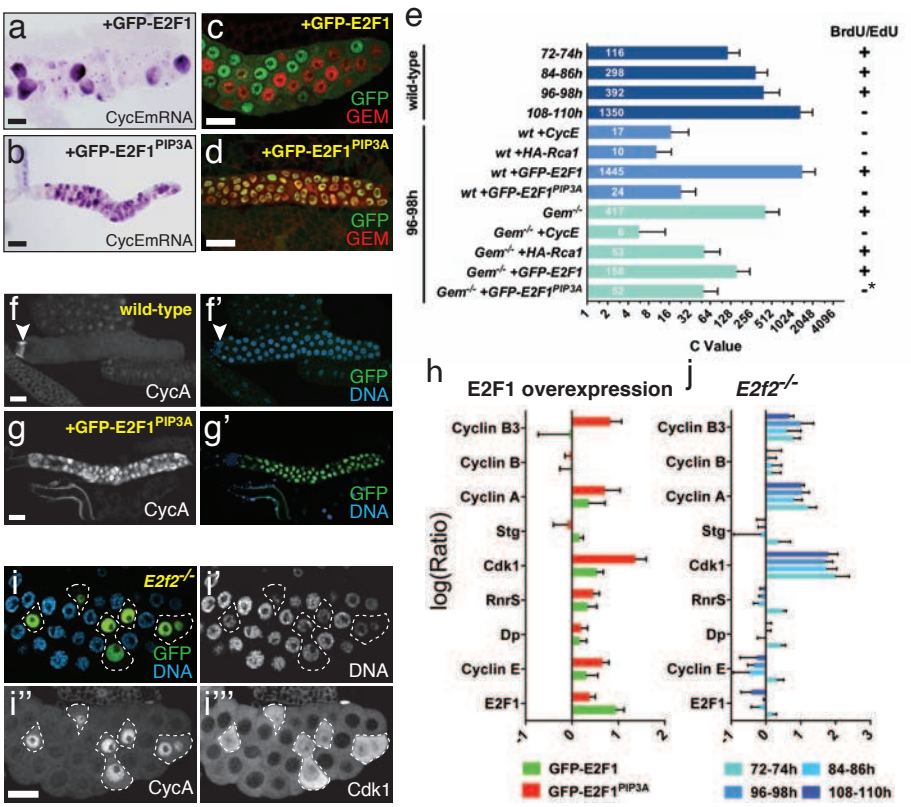
a
+GFP-E2F1
CycEmRNA
b
+GFP-E2F1PIP3A
CycEmRNA
c
+GFP-E2F1
GFP
GEM
d
+GFP-E2F1PIP3A
GFP
GEM
e
BrdU/EdU
wild-type
96-98h
72-74h
84-86h
96-98h
108-110h
wt +CycE
wt +HA-Rca1
wt +GFP-E2F1
wt +GFP-E2F1PIP3A
Gem-/-
Gem-/- +CycE
Gem-/- +HA-Rca1
Gem-/- +GFP-E2F1
Gem-/- +GFP-E2F1PIP3A
116
298
392
1350
17
10
1445
24
417
6
53
158
32
+
+
+
-
-
-
+
-
+
-
+
+
-*
1
2
4
8
16
32
64
128
256
512
1024
2048
4096
C Value
f
wild-type
CycA
f'
GFP
DNA
g
+GFP-E2F1PIP3A
CycA
g'
GFP
DNA
h
E2F1 overexpression
log(Ratio)
Cyclin B3
Cyclin B
Cyclin A
Stg
Cdk1
RnrS
Dp
Cyclin E
E2F1
-1
0
1
2
GFP-E2F1
GFP-E2F1PIP3A
i
E2f2-/-
GFP
DNA
i'
DNA
i''
CycA
i'''
Cdk1
j
E2f2-/-
Cyclin B3
Cyclin B
Cyclin A
Stg
Cdk1
RnrS
Dp
Cyclin E
E2F1
-1
0
1
2
3
72-74h
84-86h
96-98h
108-110h

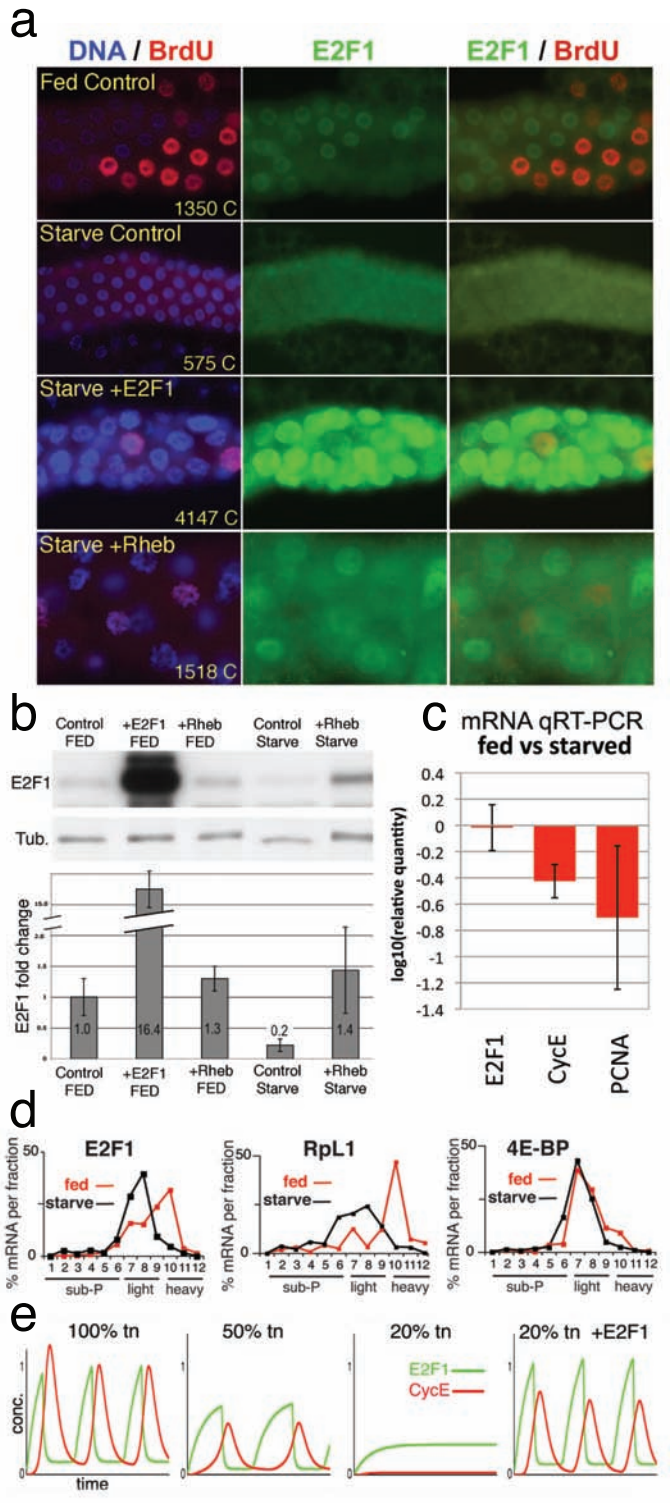
a
DNA / BrdU
E2F1
E2F1 / BrdU
Fed Control
1350 C
Starve Control
575 C
Starve +E2F1
4147 C
Starve +Rheb
1518 C
b
Control FED
+E2F1 FED
+Rheb FED
Control Starve
+Rheb Starve
E2F1
Tub.
E2F1 fold change
1.0
16.4
1.3
0.2
1.4
c
mRNA qRT-PCR
fed vs starved
log10(relative quantity)
E2F1
CycE
PCNA
d
E2F1
RpL1
4E-BP
fed
starve
% mRNA per fraction
sub-P
light
heavy
e
100% tn
50% tn
20% tn
20% tn +E2F1
E2F1
CycE
conc.
time

Control of *Drosophila* endocycles by E2F and CRL4^{Cdt2}: Supplementary Information

Norman Zielke[1,2]*, Kerry J. Kim[3]*, Vuong Tran[2]*, Shusaku T. Shibutani[5], Maria-Jose Bravo[2], Sabarish Nagarajan[6], Monique van Straaten[1], Brigitte Woods[2], George von Dassow[3], Carmen Rottig[4], Christian F. Lehner[4], Savraj Grewal[6], Robert J. Duronio[5], and Bruce A. Edgar[1,2,7]

[1]German Cancer Research Center (DKFZ)-Zentrum für Molekulare Biologie der Universität Heidelberg (ZMBH) Alliance, Im Neuenheimer Feld 282, 69120 Heidelberg, Germany

[2]Fred Hutchinson Cancer Research Center, 1100 Fairview Avenue North, Seattle, WA 98109, USA

[3]Center for Cell Dynamics, Friday Harbor Labs, University of Washington, 620 University Rd., Friday Harbor, WA 98250, USA

[4]Zoologisches Institut, Universität Zürich, Winterthurerstr. 190, 8057 Zürich, Switzerland

[5]Department of Biology, University of North Carolina, Chapel Hill, NC 27599, USA

[6]Clark H. Smith Brain Tumor Center, Southern Alberta Cancer Research Institute, and Department of Biochemistry and Molecular Biology, University of Calgary, 3330 Hospital Drive, Calgary, Alberta, T2N 4N1, Canada

[7]Corresponding Author

*These authors contributed equally to this work.

Contents

1. Supplementary Experimental Methods

Generation of *ago* mutant cells

ago^{1} loss of function clones were generated in the salivary placode using mitotic recombination. *w; FRT80B ago*^{1}*/TM6B* males were crossed to *y,w, hs-FLP*$^{1.22}$*; FRT80B P[mini-w], P[Ubi- GFP]/TM6B*^{1} females. Embryos were collected on grapejuice plates for 8h at 25°C and subsequently heat-shocked for 1.5h at 37°C. Heat-shocked samples were cultivated 96h at 25°C and then analysed by immunohistochemistry. Primary antibodies were used in the following dilutions: guinea pig-anti-CycE (1:500-800; gift of T. Orr-Weaver, Whitehead Institute, Cambridge, MA, USA), guinea pig-anti-E2F1 (1:500, T. Orr-Weaver) and mouse-anti-MPM-2 (1:200, Millipore).

Generation of *cdk2* mutant cells

Cdk2 mutant glands were generated using the genotype: *F4-Gal4 UAS-GFP/+; Cdk2FRT Cdk2*^{3}*/Cdk2*^{2} or *F4-Gal4 UAS-GFP/UAS-Flp; Cdk2FRT Cdk2*^{3}*/Cdk2*^{2}*,* where *Cdk2FRT* is a transgene encoding an Flp-excisable Cdk2. With this genotype, the animals are functionally *Cdk2*$^{+}$due to the presence of the *Cdk2FRT* transgene. In the salivary glands, however, *F4-Gal4* activates *UAS-Flp,* and Flp recombinase excises the *Cdk2FRT* wildtype Cdk2 gene from the chromsomes, making all salivary gland cells *Cdk2*^{3}*/Cdk2*^{3} mutant.

Size and DNA-measurement of *dap* mutants

Salivary glands were dissected in Ringer's solution and freed of much fat body as possible. The dissected salivary glands were then dissociated for 10 min in lysis buffer (0.5% SDS/TE). After centrifugation for 1 min at 14000 rpm, samples were incubated for 4 min with PicoGreen diluted 1:200 in TE. The fluorescence was then quantified using a flourometer (LS50B; Perkin Elmer) with an excitation-wavelength of 480 nm and an emission-wavelength of 524 nm. DNA was quantified using a calibration curve (0-150 ng) based on the DNA-Molecular Weight Marker III (Roche). To measure the area of whole larvae or dissected salivary glands, samples where mounted in 87% glycerol and imaged with a cooled CCD camera (AxioCam; Zeiss). Images were captured and analyzed using IPLab software (Signal Analytics).

Analysis of embryo extracts by western blotting

Embryos were collected for 2h at 25˚C. After incubation for 7h 25˚C, embryos were dechorionated and then homogenized in Lämmlibuffer. Salivary glands were dissected in Ringer's solution or PBS, and most of the attached fat body was removed. The glands were homogenized in Lämmlibuffer and analyzed by western blotting. Extracts were separated by SPS-PAGE and transferred to PVDF membranes (Immobilon-FL; Millipore) following standard methods. Blots were stained with Ponceau S and then probed with following primary antibodies: rabbit-anti-E2F1 (1:5000[2]); rabbit-anti-Dacapo (1:5000[3]); mouse-anti-α-tubulin (1:3000; Sigma); mouse-anti-α-tubulin (1:10000; Developmental Studies Hybridoma Bank #12G10). Appropriate HRP-coupled secondary antibodies purchased from Jackson Immunolabs were diluted 1:10000. Proteins were visualized using the ECL-Western blotting detection system (Amersham).

Comparison of Dp protein levels by western blotting

Embryos were collected for 2h at 25˚C on grape juice plates, aged for about 24h and then transferred into vials with standard fly food. At the indicated time points about 30 salivary glands were dissected in PBS and subsequently lysed in 1x RIPA (Cell Signaling Technology). The lysates were immediately frozen in liquid nitrogen and stored until usage at -80˚C. Multiple samples of each genotype were pooled and the amount of total protein was then determined with the BCA protein assay kit (Pierce). Equal amounts of protein were supplemented with Lämmlibuffer and loaded on a 10% SDS-Gel. The separated proteins were subsequently transferred to PVDF membranes (Immobilon-FL; Millipore). Blots were stained with Ponceau S and then probed with following primary antibodies: rabbit-anti-Dp (1:5000, gift from Nick Dyson, Massachusetts General Hospital, Boston, USA); rat-anti-HA (1:1000, Roche); mouse-anti-α-tubulin (1:5000; Sigma). Appropriate IR-Dye coupled secondary antibodies were purchased from Rockland Immunochemicals and diluted 1:10000. Relative protein amounts were determined with the Odyssey Infrared Imaging System (Li-Cor).

Primers

UPL assays used for qRT-PCR

Gene	Primer	UPL Probe	Transcripts
Actin 5C	agacaccaaaccgaaagacttaat acatgccagagccgttgt	#132	Act5C-RA; Act5C-RB; Act5C-RC; Act5C-RD
Cdk1	catcaaccgcgatcagaga gcggttctcctccatcaa	#88	Cdc2-RA
Cdk2	gcgcacgaactcataatgtc gaagtaagcgtgctgcagtg	#102	Cdc2c-RA; Cdc2c-RB
Cyclin A	tatttccgggagagcgaga acctcaaccagccaatcaat	#58	CycA-RA; CycA-RB
Cyclin B	gaccactgtagaacccactaaagtt ttggtcagcgacttcttcg	#56	CycB-RA; CycB-RB; CycB-RC; CycB-RD
Cyclin B3	gccaagttgcagcaaaagac ctctgggagtgtcagcaaca	#5	CycB3-RA
Cyclin E	acaaatttggcctgggacta ggccataagcacttcgtca	#43	CycE-RA; CycE-RB; CycE-RC; CycE-RD; CycE-RE
Dp	ccgcaaattcgacagagac cgcaacatttcgtttttctg	#81	dDP-RA; dDP-RB
E2F1	gctcaacgtggatctcttcaa cgccttcacgtaaatctcg	#44	E2F-RA; E2F-RB; E2F-RC
GAPDH1	gctccgggaaaaggaaaa tccgttaattccgatcttcg	#102	GAPDH1-RA
PCNA	agccaccatcctgaagaaga gtcgctgcaatcgaaggta	#147	PCNA-RA
RnrS	ccatccagtaccacgacatct caaatccacctcctcgacag	#30	RnrS-RA

Stg	cagcatggattgcaatatcagta caacgtcgtcgtcgtagaac	#17	Stg-RA

Gene-specific primers were designed with ProbeFinder software (Roche).

QuantiTect Primer Assays used for qRT-PCR

Gene	QuantiTect Primer Assay	Transcripts	Amplicon length
Cyclin E	QT01087940	cycE-RA	93bp
Dp	QT00945819	dp-RA	102bp
E2F1	QT00979931	E2F-RA; E2F-RB; E2F-RC RA:RB:RC	83bp
PCNA	QT00950769	mus209-RA	94bp

Primers for Polysome profiling

Gene	Primer
4E-BP	GCTAAGATGTCCGCTTCACC CCTCCAGGAGTGGTGGAGTA
RPL1	TGGCCTCATCAAACATCAAA AAAAGGTTTGCCAACGTCAC
E2F1	CTTCCTCTGCCATGACACCT TATTCAGGCTGGGACTGCTT

2. Supplementary Computational Methods:

The endocycle network

Oscillations in E2F1 and CycE protein levels arise from a complex network of interactions summarized in Fig S4. Here we describe our assumptions and the qualitative details of these interactions as implemented in the mathematical model. In this section, capitalized gene names refer to proteins, E2F1 refers to the active E2F1/Dp protein dimer, Cul4 is the $CRL4^{Cdt2}$ complex, Dup is Dup/Cdt1 and CycE is Cyclin E/Cdk2.

Briefly, our model tracks the concentrations of the following proteins: E2F1, Rbf, CycE, Gem, Dup, their dimers (E2F1/Rbf and Dup/Gem), and the fraction of APC^{fzr} and $CRL4^{Cdt2}$ that are active. The model also tracks the fraction of ORIs that are unlicensed, licensed (in a PreRC), and actively replicating (*i.e.* in S-phase). The mRNA concentrations from constitutively transcribed genes rapidly approach an unchanging steady state, and we assume a constant rate of synthesis of constitutively produced proteins.

Generation of E2F1 and CycE oscillations:

The *e2f* gene encodes a transcription factor that regulates many cell cycle genes. In our model, we assume E2F1 protein is synthesized at a constant rate. E2F1 associates with Dp, which is required for its activity. We do not explicitly model levels of Dp protein, and assume it is present in excess so that all E2F1 protein is immediately active upon synthesis. E2F1 is a powerful regulator of CycE transcription with regulation as follows: We assume CycE is transcribed at a low basal rate in the absence of E2F1. Free E2F1 increases the rate of CycE transcription, while E2F1/Rbf dominantly inhibits transcription (i.e. high levels of E2F1/Rbf will block all CycE transcription). Rbf protein, like E2F1, is constitutively produced at a constant rate. The effects of E2F2 and Rbf2 are not included in our model because too little is known about their regulation and interactions to include them meaningfully. Our model incorporates an explicit time delay between transcriptional activation of CycE transcription and the appearance of active CYCE protein because there is a temporal delay that arises from transcription, translation, and transport.

CycE is a key regulator of the endocycle, and is key for periodic expression of E2F1 and CycE. CycE protein can indirectly influence its own expression through Rbf. When CycE is present at high levels; it phosphorylates Rbf and dramatically lowers its affinity for E2F1, resulting in release of bound E2F1. We assume there is a slow, continuous dephosphorylation of phosphorylated RBF and that newly synthesized Rbf protein is not phosphorylated. Additionally, at high levels, CycE triggers the firing of PreRC complexes to initiate S-phase that in turn activate $CRL4^{Cdt2}$. Cul4 rapidly degrades E2F1 (and Dup, described below), and we assume $CRL4^{Cdt2}$ is inactivated at a constant rate after S-phase is complete.

These interactions generate E2F1/CycE oscillations as follows: At the start of G-phase, E2F1 and CycE levels are low. E2F1 is synthesized and begins to accumulate (some binds Rbf) and eventually results in CycE transcription and accumulation of CycE protein. This CycE protein phosphorylates Rbf and causes it to release its bound E2F1, producing additional CycE transcriptional activation. Once CycE levels are high enough,

S-phase is triggered and $CRL4^{Cdt2}$ degrades E2F1. In the absence of E2F1 activation, CycE protein levels fall during S-phase, returning the E2F1 and CycE concentrations to low levels by the start of the next G-phase.

Regulation of licensing and S-phase:

At the start of G-phase, the ORIs are in an unlicensed state, and the PreRC complex must be assembled before replication can begin. For simplicity, our model requires only Dup for PreRC formation, as Dup is required for PreRC formation in endocycling cells. We assume Dup is constitutively synthesized at a constant rate, and binds to unlicensed ORCs to form the PreRC complex. These PreRC complexes are then 'fired' by high levels of CycE at the start of S-phase. After a fixed delay (to represent the time for DNA replication), the ORIs return to the unlicensed state.

However, licensing (PreRC formation) and S-phase are usually separate processes that do not temporally overlap. Gem protein inhibits Dup by binding to it so it cannot be incorporated into the PreRC, and Gem is present at high levels during S-phase due to CycE activity: APC^{fzr} degrades Gem protein while it is active during G-phase. During S-phase, APC^{fzr} is phosphorylated and inactivated by CycE/Cdk2, allowing Gem to accumulate. Phosphorylation of Fzr and consequential inactivation by CycE/Cdk2 has been directly demonstrated with mammalian cells[4], though not in *Drosophila*[5], where the evidence is indirect[6]. Additionally, S-phase activates $CRL4^{Cdt2}$ that degrades Dup (both free Dup or Dup bound to Gem). This regulation of PreRC formation ensures that PreRC formation is allowed during G-phase when CycE is low, but during S-phase the PreRCs are fired and relicensing is not allowed until after S-phase is complete.

Modeling tools

We translated the interactions shown in Fig S4 into a system of delay differential equations that tracked the time evolution of the concentrations of endocycle network gene products (mRNA and proteins). These equations were numerically solved in Mathematica Version 5.2 (Wolfram Research). The network is available as a Mathematica notebook file upon request or from: http://celldynamics.org/celldynamics/downloads/simCode/Endocycle.zip

Mathematical approach

In this section we describe the mathematical details of our implementation of the endocycle model. Each equation in the endocycle model expresses the rate of change for a given biomolecule concentration (mRNA, protein, ORI state, or complex) as the sum of processes representing synthesis, decay, and conversion. We assume that reactions occur in well-stirred environments and that concentration (rather than absolute number of molecules or some other quantity) determines the reaction kinetics. These equations follow the same general form described previously[7-10]. Enzymatic and transcriptional activation kinetics are modeled with sigmoidal functions[11]:

$$\Phi([A],k,\nu) = \frac{[A]^{\nu}}{\kappa^{\nu} + [A]^{\nu}} \qquad (1)$$

where [A] is the concentration of the regulator, κ is the regulator concentration at which the reaction proceeds at half the maximal rate, and ν is the apparent cooperativity. This

formalism allows us to capture the envelope of possible activation curves. As described in the results section below, the ability of the endocycle network to reproduce wild-type oscillations does not require precise tuning of these parameters, indicating these oscillations do not hinge upon our specific choice of parameterization.

We were interested in relative changes in protein levels, not the absolute concentrations or changes on an absolute time scale. Maximal transcriptional and translational rates (C_e, L_e, etc.) changed only the scaling of the concentrations; these parameters could be constrained allowing us to reduce the number of free parameters while still exploring the full dynamic behavior of the network. The maximum transcriptional and translational synthesis rates were fixed at the reciprocal of the mean lifetimes when we searched for parameter sets that could reproduce lifelike behavior. Specifically, we set:

$$C_x = \frac{1}{H_x} \tag{2a}$$

$$L_x = \frac{1}{H_X} \tag{2b}$$

Where C_x is the transcription rate of gene x, L_x is the translation rate, H_x is the mean lifetime of the transcript and H_X is the mean lifetime of the protein. This amounted to a partial nondimensionalization that normalizes concentrations to their maximal steady state as described previously7,8,11,12. The concentrations of E2F1 protein, CycE mRNA, and CycE protein followed this scheme; Rbf, Dup and Gem proteins were allowed to vary over a larger range to allow for the possibility of stoichiometric differences between dimerizing partners (*i.e.* a molar excess of Rbf over E2F1). Maximal synthesis rates appear explicitly in the model (as opposed to completely removing them by nondimensionalization) because they allowed us to easily simulate the effects of gene dosage changes.

Time delays

Our model incorporated two fixed time delays. The first delay was in CycE transcription and translation to capture the temporal delay between the initiation of CycE transcription and the appearance of the CycE protein. The second was a time delay between the initiation of S-phase when PreRC's were fired by CycE and the completion of replication. We included delays because they can strongly affect the behavior of oscillators13. Based on the CycE gene and transcript lengths, and on estimates of the transcription and translation elongation rates and transport/processing times, we estimate these delays at tens of minutes14,15 or about 5-20% of a cycle. We allowed a longer period for the S-phase delay, as experiments indicate that S-phase lasts about 1/3 of the cycle. The form of the model allows for S-phase to end prior to the loss of CycE if DNA is replicated quickly, but in cases where CycE levels drop during S-phase, the loss of CycE will end S-phase. This latter scenario was suggested to occur in nurse cell endocycles by Lilly and Spradling16, and to account for under-replication of heterochromatin.

Delays were implemented as described17. Briefly, the delayed concentration $\left[\mathrm{X}(t-\Delta t)\right]$ was calculated from the non-delayed concentration $\left[\mathrm{X}(t)\right]$ using a cascade of N equations to produce a fixed delay of Δt using

$$[X(t-\Delta t)] \approx [delX_N(t)] \quad (3)$$

with

$$\frac{[delX_1(t)]}{dt} = \frac{N([delX_1(t)]-[X(t)])}{\Delta t} \quad (3a)$$

$$\frac{[delX_{n+1}(t)]}{dt} = \frac{N([delX_{n+1}(t)]-[delC_n(t)])}{\Delta t} \quad (3b)$$

where $[delX_1(t)]$ is approximately $\left[X_1(t-\frac{\Delta t}{N})\right]$, $n = 1,2,\cdots,N$ and each successive $[delX_n(t)]$ is further delayed by $\frac{\Delta t}{N}$:

$$[delX_n(t)] \approx \left[X(t-\frac{n\Delta t}{N})\right] \quad (3c)$$

Equation 3 approximates a sequential process where a molecule transitions between many intermediates. Fig S5 shows a plot of CycE mRNA and its delayed versions that correspond elongating mRNA of increasing lengths. Our method of implementing a delay is similar to a series of lowpass filters, and results in a slight attenuation of high frequencies, with the filtering becoming more severe as *N* decreases. Biologically, some lowpass filtering is expected due to the stochastic nature of elongation and transport, so Equation 3 is more realistic than a pure fixed time delay. We set *N* high enough so that it did not alter the behavior of our model: we used a cascade with $N = 10$, and models with higher *N* required more computer time to calculate but did not produce altered hit rates or change the ability of the model to reproduce experiment.

Endocycle model equations

The full mathematical model is shown below. For visual clarity, parameters are italicized; concentrations of molecules (dependent variables) are not italicized and are enclosed by brackets. Concentrations of mRNAs are lowercase, and their corresponding proteins are in uppercase. RBFp is phosphorylated Rbf, ER is the E2F1/Rbf heterodimer, ERp is the E2F1/RBFp heterodimer, and GD is the Gem/Dup heterodimer. CUL and APC refer to the fraction of active $CRL4^{Cdt2}$ and APC^{fzr} respectively, and vary from 0-1. We assume that $CRL4^{Cdt2}$ and APC are long-lived complexes that cycle between active & inactive forms. The values of U, PreRC, and S represent the fraction of ORIs that are unlicensed, licensed, and in S-phase, respectively; their sum is always 1. When time delays are present, we explicitly write the time dependence (and delay). All concentrations are initially 0 except for U and APC, which are initially 1 (i.e. all RCs are fully unlicensed and all APC is active). Perturbing these initial conditions over biologically reasonable values did not alter the steady state model behavior. Parameters are defined in Table S1. Table S1 also gives the parameter values used to generate all model output plots in the main paper and supplement.

Notation:

C_x = Transcription rate of x

L_x = Translation rate of X

κ_{Xy} = Half maximal activity of X on Y

ν_{Xy} = Cooperativity (Hill coefficient) of X on Y

K_{XY} = Dimerization on/off rate of X and Y

r_{Xy} = Maximal rate of process regulated by X on target Y

H_X = Mean lifetime of X

$\Psi = 1 - \Phi$

$$\frac{d[\mathrm{E2F}]}{dt} = L_e + K_{ER}[\mathrm{ER}] + K_{ERp}[\mathrm{ERp}] - r_{CULe}[\mathrm{E2F}]\,\Phi([\mathrm{CUL}],\kappa_{CULe},\nu_{CULe}) - K_{RE}[\mathrm{E2F}][\mathrm{RBF}] - \frac{[\mathrm{E2F}]}{H_E} \tag{4}$$

$$\frac{d[\mathrm{RBF}]}{dt} = L_r - r_{Cr}[\mathrm{RBF}]\,\Phi([\mathrm{CYCE}],\kappa_{Cr},\nu_{Cr}) + K_{ER}[\mathrm{ER}] - K_{RE}[\mathrm{E2F}][\mathrm{RBF}] + r_{Dr}[\mathrm{RBFp}] - \frac{[\mathrm{RBF}]}{H_R} \tag{5}$$

$$\frac{d[\mathrm{RBFp}]}{dt} = r_{Cr}[\mathrm{RBF}]\,\Phi([\mathrm{CYCE}],\kappa_{Cr},\nu_{Cr}) + K_{ERp}[\mathrm{ERp}] - r_{Dr}[\mathrm{RBFp}] - \frac{[\mathrm{RBFp}]}{H_R} \tag{6}$$

$$\frac{d[\mathrm{ER}]}{dt} = K_{RE}[\mathrm{E2F}][\mathrm{RBF}] + r_{Dr}[\mathrm{ERp}] - r_{Cr}[\mathrm{ER}]\;\Phi([\mathrm{CYCE}],\kappa_{Cr},\nu_{Cr}) - K_{ER}[\mathrm{ER}] - \frac{[\mathrm{ER}]}{H_R} \tag{7}$$

$$\frac{d[\mathrm{ERp}]}{dt} = r_{Cr}[\mathrm{ER}]\;\Phi([\mathrm{CYCE}],\kappa_{Cr},\nu_{Cr}) - r_{Dr}[\mathrm{ERp}] - K_{ERp}[\mathrm{ERp}] - \frac{[\mathrm{ERp}]}{H_R} \tag{8}$$

$$\frac{d[\mathrm{cyce}]}{dt} = C_c\,\Psi([\mathrm{ER}],\kappa_{Rc},\nu_{Rc})\left(\frac{(1-C_{Cc})\left(\frac{[\mathrm{E2F}]}{\kappa_{Ec}}\right)^{\nu_{Ec}}}{\left(\frac{[\mathrm{E2F}]}{\kappa_{Ec}}\right)^{\nu_{Ec}} + \left(\frac{[\mathrm{ER}]}{\kappa_{Rc}}\right)^{\nu_{Rc}} + 1} + C_{Cc}\right) - \frac{[\mathrm{cyce}]}{H_c} \tag{9}$$

$$\frac{d[\mathrm{CYCE}]}{dt} = L_c[\mathrm{cyce}(t-\Delta t_C)] - \frac{[\mathrm{CYCE}]}{H_C} \tag{10}$$

$$\frac{d[\mathrm{APC}]}{dt} = r_A(1-[\mathrm{APC}]) - r_{Ca}[\mathrm{APC}]\Phi([\mathrm{CYCE}],\kappa_{Ca},\nu_{Ca}) \tag{11}$$

$$\begin{aligned}\frac{d[\mathrm{GEM}]}{dt} = {} & L_g + K_{DG}[\mathrm{GD}] + \frac{[\mathrm{GD}]}{H_D} + r_{CULd}[\mathrm{GD}]\Phi([\mathrm{CUL}],\kappa_{CULd},\nu_{CULd}) - K_{GD}[\mathrm{GEM}][\mathrm{DUP}] \\ & - r_{Ag}[\mathrm{GEM}]\Phi([\mathrm{APC}],\kappa_{Ag},\nu_{Ag}) - \frac{[\mathrm{GEM}]}{H_G}\end{aligned} \tag{12}$$

$$\begin{aligned}\frac{d[\mathrm{DUP}]}{dt} = {} & L_d + K_{DG}[\mathrm{GD}] + r_{Ag}[\mathrm{GD}]\Phi([\mathrm{APC}],\kappa_{Ag},\nu_{Ag}) - K_{UD}[\mathrm{U}][\mathrm{DUP}] - K_{GD}[\mathrm{GEM}][\mathrm{DUP}] \\ & - r_{CULd}[\mathrm{DUP}]\Phi([\mathrm{CUL}],\kappa_{CULd},\nu_{CULd}) - \frac{[\mathrm{DUP}]}{H_D}\end{aligned} \tag{13}$$

$$\begin{aligned}\frac{d[\mathrm{GD}]}{dt} = {} & K_{GD}[\mathrm{GEM}][\mathrm{DUP}] - K_{DG}[\mathrm{GD}] - r_{CULd}[\mathrm{GD}]\Phi([\mathrm{CUL}],\kappa_{CULd},\nu_{CULd}) \\ & - r_{Ag}[\mathrm{GD}]\Phi([\mathrm{APC}],\kappa_{Ag},\nu_{Ag}) - \frac{[\mathrm{GD}]}{H_G} - \frac{[\mathrm{GD}]}{H_D}\end{aligned} \tag{14}$$

$$\frac{d[\mathrm{CUL}]}{dt} = r_{Sc}(1-[\mathrm{CUL}])\Phi([\mathrm{S}],\kappa_{Sc},\nu_{Sc}) - \frac{[\mathrm{CUL}]}{H_{CUL}} \tag{15}$$

$$\frac{d[\mathrm{U}]}{dt} = r_{Cs}[\mathrm{PreRC}(t-\Delta t_S)]\Phi([\mathrm{CYCE}(t-\Delta t_S)],\kappa_{Cs},\nu_{Cs}) - K_{UD}[\mathrm{U}][\mathrm{DUP}] \quad (16)$$

$$\frac{d[\mathrm{PreRC}]}{dt} = K_{UD}[\mathrm{U}][\mathrm{DUP}] - r_{Cs}[\mathrm{PreRC}]\Phi([\mathrm{CYCE}],\kappa_{Cs},\nu_{Cs}) \quad (17)$$

$$[\mathrm{S}] = 1 - [\mathrm{U}] - [\mathrm{PreRC}] \quad (18)$$

Equations in endocycle model variants:

We also explored several model variants shown in Fig S4 that implemented additional or alternative regulation and modified the system of equations. These are described in the paragraphs below.

Models allowing E2F1 to regulate transcription of Dup (cyan lines). Replace Equation 12 with:

$$\frac{d[\mathrm{dup}]}{dt} = C_d\Psi([\mathrm{ER}],\kappa_{Rd},\nu_{Rd})\left(\frac{(1-C_{Cd})\left(\frac{[\mathrm{E2F}]}{\kappa_{Ed}}\right)^{\nu_{Ed}}}{\left(\frac{[\mathrm{E2F}]}{\kappa_{Ed}}\right)^{\nu_{Ed}} + \left(\frac{[\mathrm{ER}]}{\kappa_{Rd}}\right)^{\nu_{Rd}} + 1} + C_{Cd}\right) - \frac{[\mathrm{dup}]}{H_d} \quad (19)$$

$$\frac{d[\mathrm{DUP}]}{dt} = L_d[\mathrm{dup}(t-\Delta t_C)] + K_{DG}[\mathrm{GD}] + r_{Ag}[\mathrm{GD}]\Phi([\mathrm{APC}],\kappa_{Ag},\nu_{Ag}) - K_{UD}[\mathrm{U}][\mathrm{DUP}] - K_{GD}[\mathrm{GEM}][\mathrm{DUP}] - r_{CULd}[\mathrm{DUP}]\Phi([\mathrm{CUL}],\kappa_{CULd},\nu_{CULd}) - \frac{[\mathrm{DUP}]}{H_D} \quad (20)$$

Models with simplified PreRC formation (blue line) abstracted the effects of the APC/GEM activity so that CycE blocked PreRC formation directly. Here, we eliminated APC, GEM & GD (Equations 11, 12, & 14), and replaced Equations 13, 16, and 17 with:

$$\frac{d[\mathrm{DUP}]}{dt} = L_d - K_{UD}[\mathrm{U}][\mathrm{DUP}]\Psi([\mathrm{CYCE}],\kappa_{Cp},\nu_{Cp}) - r_{CULd}[\mathrm{DUP}]\Phi([\mathrm{CUL}],\kappa_{CULd},\nu_{CULd}) - \frac{[\mathrm{DUP}]}{H_D} \quad (21)$$

$$\frac{d[\mathrm{U}]}{dt} = r_{Cs}[\mathrm{PreRC}(t-\Delta t_S)]\Phi([\mathrm{CYCE}(t-\Delta t_S)],\kappa_{Cs},\nu_{Cs}) - K_{UD}[\mathrm{U}][\mathrm{DUP}]\Psi([\mathrm{CYCE}],\kappa_{Cp},\nu_{Cp}) \quad (22)$$

$$\frac{d[\mathrm{PreRC}]}{dt} = K_{UD}[\mathrm{U}][\mathrm{DUP}]\Psi([\mathrm{CYCE}],\kappa_{Cp},\nu_{Cp}) - r_{Cs}[\mathrm{PreRC}]\Phi([\mathrm{CYCE}],\kappa_{Cs},\nu_{Cs}) \quad (23)$$

In our standard model, delays from transcription and translation of CycE were combined in Equation 9. A model with separate transcriptional and translational delays (Δt_{Ctr} and Δt_{Ctl} respectively) had no change in behavior, but was slower to solve. In this model, Equations 9 and 10 are replaced by:

$$\frac{d[\mathrm{cyce}]}{dt} = C_c\Psi([\mathrm{ER}(t-\Delta t_{Ctr})],\kappa_{Rc},\nu_{Rc})\left(\frac{(1-C_{Cc})\left(\frac{[\mathrm{E2F}(t-\Delta t_{Ctr})]}{\kappa_{Ec}}\right)^{\nu_{Ec}}}{\left(\frac{[\mathrm{E2F}(t-\Delta t_{Ctr})]}{\kappa_{Ec}}\right)^{\nu_{Ec}} + \left(\frac{[\mathrm{ER}(t-\Delta t_{Ctr})]}{\kappa_{Rc}}\right)^{\nu_{Rc}} + 1} + C_{Cc}\right) - \frac{[\mathrm{cyce}]}{H_c} \quad (24)$$

$$\frac{d[\mathrm{CYCE}]}{dt} = L_c[\mathrm{cyce}(t-\Delta t_{Ctl})] - \frac{[\mathrm{CYCE}]}{H_C} \quad (25)$$

Dup may be liberated from the PreRC at the start of S-phase by CycE activity (yellow line). In this, Equation 13 was replaced with:

$$\frac{d[\mathrm{DUP}]}{dt} = L_d + K_{DG}[\mathrm{GD}] + r_{Ag}[\mathrm{GD}]\Phi([\mathrm{APC}],\kappa_{Ag},\nu_{Ag}) + r_{Cs}[\mathrm{PreRC}]\Phi([\mathrm{CYCE}],\kappa_{Cs},\nu_{Cs}) - K_{UD}[\mathrm{U}][\mathrm{DUP}] - K_{GD}[\mathrm{GEM}][\mathrm{DUP}] - r_{CULd}[\mathrm{DUP}]\Phi([\mathrm{CUL}],\kappa_{CULd},\nu_{CULd}) - \frac{[\mathrm{DUP}]}{H_D} \quad (26)$$

Finally, we explored models that allowed degradation of E2F1 in the ER and ERp complexes. Incorporating any of the changes into the model individually or in combination did not prevent the model from reproducing any of the experimentally observed behavior listed in Table S2, though they did alter the fraction of parameter sets doing so (see Supplementary Discussion).

We also explored a model where E2F1 degradation was controlled directly by CycE activity (independent of an S-phase or $CRL4^{Cdt2}$ activity). This model could produce oscillations, but overexpression of CycE always resulted in arrest with low E2F1. In this model, we replaced Equation 4 with:

$$\frac{d[\mathrm{E2F}]}{dt} = L_e + K_{ER}[\mathrm{ER}] + K_{ERp}[\mathrm{ERp}] - r_{Ce}[\mathrm{E2F}]\,\Phi([\mathrm{CYCE}],\kappa_{Ce},\nu_{Ce}) - K_{RE}[\mathrm{E2F}]\,[\mathrm{RBF}] - \frac{[\mathrm{E2F}]}{H_E} \quad (27)$$

To simulate $E2F1^{PIP3A}$, we added additional E2F1 that was not degraded by $CRL4^{Cdt2}$ but otherwise behaved identically to E2F1. Equations 5, 6 and 9 were altered, and we added E2Fp, the nondegradable E2F1 as described below:

$$\frac{d[\mathrm{RBF}]}{dt} = L_r - r_{Cr}[\mathrm{RBF}]\,\Phi([\mathrm{CYCE}],\kappa_{Cr},\nu_{Cr}) + K_{ER}[\mathrm{ER}] + K_{ER}[\mathrm{EpR}] - K_{RE}[\mathrm{E2F}][\mathrm{RBF}] - K_{RE}[\mathrm{E2Fp}][\mathrm{RBF}] + r_{Dr}[\mathrm{RBFp}] - \frac{[\mathrm{RBF}]}{H_R} \quad (28)$$

$$\frac{d[\mathrm{RBFp}]}{dt} = r_{Cr}[\mathrm{RBF}]\,\Phi([\mathrm{CYCE}],\kappa_{Cr},\nu_{Cr}) + K_{ERp}[\mathrm{ERp}] + K_{ERp}[\mathrm{EpRp}] - r_{Dr}[\mathrm{RBFp}] - \frac{[\mathrm{RBFp}]}{H_R} \quad (29)$$

$$\frac{d[\mathrm{cyce}]}{dt} = C_c\,\Psi([\mathrm{ER}]+[\mathrm{EpR}],\kappa_{Rc},\nu_{Rc})\left(\frac{(1-C_{Cc})\left(\frac{[\mathrm{E2F}]+[\mathrm{E2Fp}]}{\kappa_{Ec}}\right)^{\nu_{Ec}}}{\left(\frac{[\mathrm{E2F}]+[\mathrm{E2Fp}]}{\kappa_{Ec}}\right)^{\nu_{Ec}} + \left(\frac{[\mathrm{ER}]+[\mathrm{EpR}]}{\kappa_{Rc}}\right)^{\nu_{Rc}} + 1} + C_{Cc}\right) - \frac{[\mathrm{cyce}]}{H_c} \quad (30)$$

$$\frac{d[\mathrm{E2Fp}]}{dt} = L_{ep} + K_{ER}[\mathrm{EpR}] + K_{ERp}[\mathrm{EpRp}] - K_{RE}[\mathrm{E2Fp}]\,[\mathrm{RBF}] - \frac{[\mathrm{E2Fp}]}{H_E} \quad (31)$$

$$\frac{d[\mathrm{EpR}]}{dt} = K_{RE}[\mathrm{E2Fp}][\mathrm{RBF}] + r_{Dr}[\mathrm{EpRp}] - r_{Cr}[\mathrm{EpR}]\,\Phi([\mathrm{CYCE}],\kappa_{Cr},\nu_{Cr}) - K_{ER}[\mathrm{EpR}] - \frac{[\mathrm{EpR}]}{H_R} \quad (32)$$

$$\frac{d[\mathrm{EpRp}]}{dt} = r_{Cr}[\mathrm{EpR}]\,\Phi([\mathrm{CYCE}],\kappa_{Cr},\nu_{Cr}) - r_{Dr}[\mathrm{EpRp}] - K_{ERp}[\mathrm{EpRp}] - \frac{[\mathrm{EpRp}]}{H_R} \quad (33)$$

3. Supplementary Discussion

Finding working parameter sets

The behavior of our model depended on the parameters governing the interactions within the model, none of which have been experimentally measured. To investigate whether our model could reproduce wild-type oscillations, we randomized all free parameters within biologically plausible ranges, and searched for sets of parameter values that reproduced the observed salient features of wild-type oscillations (described below). The range of parameter values used in our search is shown in Table S1. We chose wide ranges (usually one or two orders of magnitude) to fully explore the biologically reasonable range of parameter values7. Additional constraints were placed on some parameter values to reflect our knowledge of the system:

(1) $CRL4^{Cdt2}$ activity rapidly degraded E2F1 and Dup, with at least a 5-fold increase in degradation over basal rates ($r_{CULe} > \frac{5}{H_e}$ and $r_{CULd} > \frac{5}{H_d}$).

(2) Similarly, APC^{fzr} rapidly degraded Gem, with at least a 5-fold increase in degradation over basal rates ($r_{Ag} > \frac{5}{H_g}$).

(3) The complex of E2F1 bound to phosphorylated Rbf had a much faster dissociation rate than when bound to non-phosphorylated Rbf ($K_{ERp} > 5K_{ER}$).

(4) Gem bound Dup with high affinity, with an on rate at least 10x faster than the off rate ($K_{GD} > 10K_{DG}$) and at least 5x faster than the binding of Dup to the PreRC($K_{GD} > 5K_{ND}$).

(5) Cooperativities were restricted to integer values. This does not reflect a biological constraint, but numerical solving of our system was much faster with integer cooperativities. Searches allowing non-integer cooperativities did not change our results or conclusions.

Asserting the above constraints served to speed the search for lifelike oscillations; relaxing the constraints above merely resulted in a lower frequency of finding working parameter sets. We considered a set of parameter values acceptable if the model reproduced salient features of wild-type (WT) oscillations, as follows:

(1) **Large amplitude oscillations in E2F1, Gem and CycE protein levels**: All of these had to have at least a 4-fold change over the course of a cycle. This was consistent with quantification of the nuclear signal from Fig 1 that showed these proteins had dramatic changes in cycling cells.

(2) **Non-overlapping, narrow E2F1 & CycE peaks:** E2F1 and CycE were not simultaneously maximal (*i.e.* when one is at its maximal value, the other must be below half its maximal value), and E2F1 peaked prior to CycE in each cycle, as shown by the phase plots in Fig 1. Consistent with quantification of nuclear expression, we also required E2F1 and CycE protein to be at high levels (greater than half maximal) for less than 40% of the cycle.

(3) **Overlapping CycE and Gem peaks:** Gem and CycE are usually expressed at high levels in the same cell. Consistent with observation, when Gem is at its maximal value we require CycE to be at least 1/3 its maximal value. Additionally, Gem is present at high levels in few cells, and we require Gem protein to be at high levels (greater than half maximal) for less than 40% of the cycle.

(4) **DNA doubling during each cycle:** PreRC formation rose above 75% during G-phase and fell below 10% by the end of S-phase. We sometimes observed cycling with only modest PreRC variation, and this is inconsistent with the apparent doubling of DNA each cycle.

Restrictions & constraints on parameters revealed by the model

We found parameter sets satisfying the above criteria. The fraction of parameter sets doing so (hereafter referred to as the hit rate) was approximately 1 in 10,000. Fig S6 shows histograms of the distribution of parameter values for 1375 parameter sets producing lifelike oscillations. For most parameters, WT oscillations were possible across the whole explored range, but some parameters had absolute restrictions where values outside of a specific range never produced WT cycles. Neglecting the effects of the constraints we imposed during our random parameter search ($K_{ERp} > 5K_{ER}$, etc), our model predicted that the following quantitative constraints were required for WT oscillations: (1) CycE transcription was steeply activated by intermediate levels of free E2F1 protein ($\nu_{Ec} > 1$ and $\kappa_{Ec} > 0.05$). The threshold for transcriptional activation of CycE by E2F1 (k_{Ec}) was not too low (or too graded), or else the basal level of free E2F1 resulted in a continuous high level of CycE transcription. (2) CycE activation of the PreRC was fast ($r_{Cp} > 0.025$) and steeply activated by intermediate levels of CycE ($\nu_{Cs} > 1$ and $\kappa_{Cs} > 0.02$). Again, if the threshold for CycE activating the PreRC was too low or graded, the basal CycE resulted in immediate firing of PreRCs after licensing. (3) The constitutive (non-E2F regulated) rate of CycE production (C_{Cc}) was very low to allow for large amplitude CycE oscillations. As the fraction of constitutively transcribed cyce rose, E2F1 had a correspondingly weaker ability to modulate CycE activity, and the amplitude of CycE oscillations fell.

It is possible that the large range of working parameter values is due to compensation where a particularly large value for one parameter is balanced by a reduced value in another. To test the extent of compensation between pairs of parameter values, we measured the Pearson product-moment cross correlation coefficient (ρ) between all pairs of parameters, shown in Fig S7. Neglecting correlations due to constraints between parameters we imposed during our search (i.e. $K_{ERp} > 5K_{ER}$, etc.), no pair of parameters showed strong correlation ($|\rho| \geq 0.4$). The lack of correlations indicates that compensation is either relatively weak or involves triplets or larger groups of parameters.

The endocycle network robustly reproduces wild type oscillations

The endocycle model robustly produced wild-type oscillations despite large changes in parameter values. The histograms shown in Fig S6 show that lifelike oscillations were produced over large (1-2 orders of magnitude) ranges and with few restrictions on the range of parameter values. This hit rate for the endocycle network of 1 in 10,000 is ~2 orders of magnitude lower than that found in previous studies of the segment polarity and neurogenic networks7,9. This difference is likely attributable to the stringency of what was required of working parameter sets. In this study, our model had to make oscillations that reproduced numerous quantitative features of wild-type oscillations. When additional criteria were added to the segment polarity network (i.e. the ability to sharpen a blurred initial pattern), the hit rate fell dramatically. If the segment polarity or neurogenic networks were required to more carefully match as many quantitative features as we have required for the endocycle, their hit rates would likely fall to a comparable level.

The endocycle model reproduces the effects of many perturbations and mutations

We next challenged our model to reproduce the phenotypes of experimental perturbations of the endocycle genes. We also used our model to test whether the endocycle rate may be slowed by reducing translation rate to mimic starvation. The list of perturbations we explored is summarized in Table S2. Starting with parameter sets that reproduced wild type cycles, we simulated the perturbations in Table S2 and recorded the fraction of parameter sets satisfying each criterion. We found 12 parameter sets that satisfied all these new criteria. Fig S10 shows the model results for each of the perturbations in Table S2 that are not shown elsewhere. Some criteria were more stringent than others, and we discuss our key assumptions and findings below.

E2F1 overexpression:

Quantification of E2F1-overexpressing salivary glands showed relatively unchanged profiles of E2F1 and CycE expression. The fraction of cells with high E2F1 or high CycE did not change noticeably when E2F1 was overexpressed (compared to WT) though the level of maximal expression (peak E2F1 or CycE staining) appeared higher. Additionally, DNA quantification showed that cycling was faster. After simulating a tripling of E2F protein production, we were able to reproduce all of these qualitative features in the model that were observed in experiment.

We do not know the factor by which E2F1 protein synthesis was increased in E2F1 overexpressing glands. E2F1 mRNA was increased by a factor of ~10 as measured by qRT-PCR (Fig 3I), but it is quite possible this did not translate to a 10-fold increase in E2F1 protein, as the translational machinery may be saturated (or nonlinear) or Dp protein levels may become limiting. Thus, a 3-fold increase in E2F1 protein production is a reasonable assumption, and several parameter sets continued to reproduce observed oscillations when we simulated larger increases in E2F1 overexpression in the model.

Rbf loss/overexpression:

Rbf is a potent regulator of E2F1 activity and can arrest the endocycle when overexpressed (Fig 2), but is not required as cycling proceeds after the loss of Rbf. Our model easily reproduced these results (Fig 2). Sufficiently high Rbf was always sufficient to arrest E2F1 and CycE oscillations, as this would result in a complete block of CycE production. In the absence of Rbf, the model was able to reproduce WT oscillations and the effects of mutations (except those involving Rbf). Usually, elimination of Rbf resulted in a slight acceleration of E2F1 and CycE oscillations but otherwise normal cycling. Thus, our model suggests that Rbf regulation does not strongly shape normal cycling, and its primary function is to arrest cycling when Rbf is expressed at high levels.

CycE overexpression:

CycE overexpression was the most difficult perturbation for the model to capture (*i.e.* it had the lowest frequency of parameter sets satisfying reproducing this perturbation). We simulated the addition of constitutively overproduced CycE production in the model. Often, CycE overexpression eliminated E2F1 and CycE oscillations, but was accompanied by a low but continuous S-phase that resulted from an incomplete block of PreRC formation (*i.e.* the high CycE was not sufficient to completely block Dup through APC^{fzr} and Gem activity). We did not observe any BrdU incorporation under conditions

of CycE overexpression in experiment. The indicated fraction (2%) of parameter sets reproduced all the qualitative features of CycE overexpression.

Ago loss:

The F-box protein Archipelago (Ago/Cdc4/Fbw7), which targets CycE for degradation, is required for endocycle progression[18] (Fig S1). It has also been shown that Cyclin E can target itself for degradation by autophosphorylation[19], but the detailed regulation of this is unclear. Our model usually required unstable CycE protein (Fig S6) to reproduce wild-type oscillations. When we simulated the effects of the Ago^{1} mutation by increasing the stability of CycE protein (increasing H_C by a factor of 10), we were able to reproduce the experimentally observed arrest with high CycE.

Dp mutants:

As predicted by the computer model, loss of E2F1 essentially abolished endoreplication in the salivary gland (Fig S13). Deletion of its designated binding partner Dp might therefore be expected to result in a similar phenotype, as predicted by our model (Fig S10). It should be kept in mind however that Dp is required in both activating E2F1/Dp and repressing E2F2/Dp complexes. Experimentally, we found that *Dp* null mutant salivary gland cells had a much weaker endocycle defect than *e2f* mutant cells (Fig 2, S13, S14, S15). Endoreplication in *Dp* mutants was significantly delayed, but salivary glands showed regular, oscillating patterns of BrdU incorporation and reached normal DNA contents by about 180h AED (endoreplication in wild-type is complete and ceases at 96h AED). We observed, however, aberrant chromosome morphology in the *Dp* mutants (Fig S15), suggesting that their DNA replication may not be completely normal.

In our computer simulation, CycE oscillations were always absent whenever E2F1 or Dp were eliminated, because E2F1/Dp was the only activator of CycE expression (Fig S10). Our model, however, could produce CycE oscillations and periodic S-phases with as little as ¼ the normal amount of E2F1, while reproducing all other perturbations in Table S2. RT-qPCR showed that overall E2F target gene expression was reduced in *Dp* mutant salivary glands, but transcripts were still detectable (Fig S15). RNA *in situ* hybridization showed normal oscillation of *CycE* and *RnrS* transcripts in these mutant glands (Fig S15). We also observed normal oscillation of Geminin protein in the *Dp* mutant (Fig S15). Geminin is an APC^{fzr} target that is believed to oscillate because of the periodic repressive activity of CycE/Cdk2 on APC^{fzr}, and thus this result implies that CycE/Cdk2 activity oscillates in the *Dp* mutants. Taking these results together, the most likely explanation for continued endocycling in the *Dp* mutants is that residual Dp protein allows continued oscillations of E2F activating and repressive transcriptional activity, driving the endocycle in essentially the same way as in WT.

Western blotting experiments revealed trace amounts of Dp protein in salivary glands from *Dp* null mutants (Fig S15), and quantification of these bands indicated that *Dp* mutants contained about 8% of residual Dp protein at 96h and 120h AED (Fig S15). Since Dp is thought to be a relatively stable protein, this residual Dp is likely maternally derived. To genetically test the presence of maternally derived Dp protein, wild-type GFP-E2F1 or non-degradable E2F1 ($GFP\text{-}E2F1^{PIP3A}$) were overexpressed in *Dp* mutants (Fig S16). We found that $GFP\text{-}E2F1^{PIP3A}$ was still capable of blocking endocycle progression in *Dp* mutants, although the arrest was less stringent than in wild-type (Fig S16). Moreover, expression of non-degradable E2F1 in *Dp* mutants was associated with

severe chromosomal defects (Fig S16). In contrast, the oscillation of S-phase in *Dp* mutants was not affected significantly affected by overexpression of full-length WT (degradable) GFP-E2F1 (Fig S16). The ability of wild-type E2F1 to drive accelerated endocycling and consequent hyperpolyplody was strongly reduced in the *Dp* mutants (Fig S16), indicating that the reduced amount of Dp protein available to form E2F1/Dp complexes had limited the rate of endoreplication. Since all extant data indicate that Dp is essential for E2F1 function, we conclude that *Dp* mutants retain residual amounts of Dp protein, which are sufficient to allow slow but otherwise fairly normal endocycles in *Dp* mutants.

An important question that stills remains to be answered is whether endoreplication can occur in complete the absence of E2F/Dp activity. Since our work demonstrated that *Dp* mutants are still likely to contain functional E2F1/Dp complexes, we lack the tools to test this idea experimentally. However, we have used our model to address this question theoretically. This modeling approach suggested two possible ways in which DNA replication might be able to continue without any functional E2F. First, our model predicts the possibility of an extended, slow S-phase triggered by the basal level of CycE expression that occurs without E2F1 activation or E2F1/Rbf repression, as shown in Figure S10. In such cases, replicated DNA could be relicensed because CycE was too low to block licensing through APC^{fzr} and Gem. Table S2 shows the fraction of wild-type parameter sets with this behavior, and this continuous replication is compatible with the behavior of other mutations, as some parameter sets reproduced all perturbations in Table S2. Continuous replication, however, is not consistent with our experimental observations, which showed BrdU incorporation in only a fraction of nuclei in *Dp* mutant salivary glands (Fig S14, S16). Second, our model predicts that Dup/$CRL4^{Cdt2}$ oscillations may be possible in the complete absence of E2F1. These oscillations rely on periodic $CRL4^{Cdt2}$ activity that removes all Dup. However, such E2F1-independent oscillations were rare in our parameter search: Less than 0.01% of parameter sets that produced normal cycles (wild-type oscillations in the presence of E2F1) could also produce E2F1-independent oscillations when we simulated removal of all E2F1. Moreover, we were unable to find *any* parameter sets that produced E2F1-independent oscillations and that also reproduced all perturbations listed in Table S2. We note, however, that an E2F1-independent endocycle based on Dup←→$CRL4^{Cdt2}$ feedback interactions is theoretically possible.

$E2F1^{PIP3A}$:

To mimic the effects of $E2F1^{PIP3A}$, we simulated addition of E2F1 that was nondegradable by $CRL4^{Cdt2}$ activity (Equations 30-35). Endogenous (degradable) E2F1 was also present, but the simulated $E2F1^{PIP3A}$ (nondegradable) was expressed at twice the level in our model. The $E2F1^{PIP3A}$ rapidly accumulated (since it was not periodically degraded) and always resulted in continuously high levels of CycE expression, and a complete block of S-phase.

Loss of $CRL4^{Cdt2}$ activity:

Is it possible that periodic E2F1 degradation is not required for endocycling? To test this, we examined the behavior of the model when $CRL4^{Cdt2}$ could not degrade the endogenous E2F1, and when $CRL4^{Cdt2}$ had no activity at all (it degraded neither E2F1 nor Dup). Conceptually, E2F1 oscillations are possible in such a model, and could arise

through periodic stabilization through binding to Rbf (i.e. E2F1 is stabilized by binding to Rbf). However, we failed to find any parameter sets that reproduced wild-type E2F1 or CycE oscillations despite searching > 200 million parameter sets. This vanishingly small hit rate indicates that wild-type oscillations without $CRL4^{Cdt2}$ require exquisitely tuned kinetics (we did not perform an exhaustive search), and therefore such oscillations are unlikely to be robust to parameter changes or simulated mutation. Taken together, modeling and experiment suggests that endocycles require periodic E2F1 degradation.

Loss of APC activity and Geminin overexpression:
Periodic degradation of Gem appears to be required for normal endocycles, as Gem overexpression or loss of APC^{fzr} activity both result in cycle arrest/slowing with high E2F1 and CycE[20]. Experimentally, APC^{fzr} activity was eliminated by overexpression of the APC^{fzr} inhibitor Rca1, and we simulated this in the model by blocking the activity of APC^{fzr} (*i.e.* so it could no longer degrade Gem). We simulated Gem overexpression by increasing Gem synthesis by a factor of 10. Our model was able to reproduce the observed arrest with high E2F1 and CycE with both perturbations, consistent with experiment.

Starvation control of rate of cycling:
We simulated starvation conditions by reducing all translation rates (L parameters) by 33%, and requiring cycling continue, but at a slower rate. Our model was able to reproduce this, and with additional translation reduction, the cycle eventually arrested with no DNA replication. Our model predicts that translational throttling through 5'UTR regulation is a viable way to control the rate of cycling[21,22]. We explored the effect of individual parameters on the rate of cycling as discussed in the next section.

Sensitivity of endocycle rate to parameter changes

We systematically perturbed each model parameter to see what parameters most strongly affect the rate of cycling. We started with the 12 parameter sets that reproduced all mutations and measured the change in period when a parameter was lowered by 10% while all other parameters were held fixed. This process was repeated for all parameters, and the average fractional change in period for each perturbation was recorded. If a perturbation resulted in cycle arrest, it was excluded from the average. Fig S8 shows the average effect of a 10% reduction of each parameter on the period.

The model indicates that slowing of the cycle during starvation is mostly due to changes in the E2F1 or CycE transcriptional synthesis rates (L_e, or L_c); throttling translation of Gem, Dup and Rbf had little effect on the period. The model indicated that there are 2 additional strategies that would allow for the period to be tuned: First, slowing the global kinetics of E2F1 accumulation during G phase would slow the cycle as it would take longer to trigger CycE production. This could be accomplished by reducing the amount of E2F1 (by decreasing the mean lifetime of the E2F1 protein H_E, reducing translation L_e), or decreasing its activity (raising κ_{Ec}). Second, the endocycle could be sped by shortening S-phase (Δt_S) or its effect on $CRL4^{Cdt2}$: shortening the active lifetime of $CRL4^{Cdt2}$ (H_{CUL}), lowering the threshold for E2F1 degredation (κ_{CULe}), or lowering the threshold for $CRL4^{Cdt2}$ activation (κ_{Scul}).

Robustness of parameter sets reproducing all perturbations

To analyze the sensitivity of the model to parameter perturbation, we systematically varied individual parameters one at a time within each of 28 parameter sets that reproduced the observed effect of all mutations in Table S2. Each parameter (except for cooperativities) was varied from 0.1 to 10 times its original working value, while the other parameters were held fixed. The fraction of parameter sets that continued to produce oscillations (stable oscillations with a 2-fold change in CycE over a cycle) over at least 1 full order of magnitude is shown in Fig S9. On average, 90% of parameters could tolerate an order of magnitude variation (i.e. continue to produce oscillations over at least a 10-fold variation in the given parameter). Part of this robustness reflects the criteria in Table S2: these parameter sets must, for example, tolerate substantial E2F1 and Rbf variation, but many parameters (such as delays and activities) had no such constraints. Our model strongly suggests that the endocycle network present in cycling cells is extremely robust to parameter perturbation.

Identifying essential regulatory interactions

We also constructed variations of our model that incorporated additional or alternate regulation (see Supplementary Methods) and explored whether these models were able to continue to reproduce experiment. This allowed us to identify which regulatory features were essential for reproducing experiment; if models continued to reproduce experiment after a change to the model, then th change reflects a detail unimportant to capture lifelike behavior. Expression of Dup is possibly regulated by E2F1, and we tested whether such regulation would change the behavior of our model. Models incorporating this regulation were capable of reproducing WT oscillations and all mutant effects in Table S2, so our model indicates the specifics of Dup are not essential. We explored models were Dup was released from the PreRC at the start of S-phase and a simplified network where the effects of Gem and APC^{fzr} were abstracted by having CycE activity directly block PreRC formation. These models were also able to reproduce WT oscillations and all mutations in Table S2. These findings indicate that the ability to reproduce experiment is not an artifact of a carefully optimized network.

Some perturbations to the model eliminated its ability to reproduce all behavior. As described previously, periodic E2F1 degradation by $CRL4^{Cdt2}$ is essential for producing normal cycles. It has also been hypothesized that E2F1 is phosphorylated and destabilized by CycE. We explored a model variant where high levels of CycE, but not $CRL4^{Cdt2}$ caused degradation of E2F1, and found that it could produce normal cycles, but failed to arrest with high E2F1 when CycE was overexpressed. Taken together, our model predicts that periodic E2F1 degradation during S-phase is essential. Future models could also explore the effects of CycE degradation through autophosphorylation and Ago activity. Our model indicates these effects are not required for normal cycling, as lifelike behavior is generated without their inclusion.

Delays shaped the CycE expression during the endocycle

Our model allowed us to investigate the effects of changing the time delay in CycE production. Fig S8 indicates that the CycE transcriptional and translational delay (Δt_C) could usually be varied by an order of magnitude without disrupting cycling, indicating that the model can robustly produce lifelike oscillations regardless of the delay. One

would expect that the duration of the delay could affect the period of the endocycle; elimination of the delay would allow CycE to rise faster in response to E2F1 and lead to faster cycling. This intuition is confirmed in Fig S8 where we show that a 10% reduction in these delays resulted, on average, in a mild speeding of the cycle.

If endogenous CycE were replaced by a cDNA (with the endogenous promoters & regulator sites present but lacking introns), our model predicts that the endocycles produced may be detectably altered. Introns account for up to 2/3 of the cyce transcript[23], and so their removal may reduce the delay between transcriptional initiation and the start of translation. If we assume that the total delay is reduced by a factor of 2, our model predicts that the cycle time should always decrease, speeding the cycle by 2-8% (mean = 5%) in parameter sets that satisfy all criteria in Table S2. Such a shift, while small, could result in an additional endocycle during development and thus produce a noticeable change.

4. Supplementary Tables

Table S1: Parameters in model

All parameters in the main model are listed below. The working value was used to generate all graphs of model behavior shown in the main paper and Fig S10, perturbations to parameters to mimic experiment are detailed in Table S2. These parameters have not been experimentally measured, so we used a Monte-Carlo search over the specified range and sampling distribution shown.

Symbol	Description	Working Value	Range, sampling for Random Search
	CycE transcriptional regulation:		
κ_{Ec}	E2F1 concentration for half maximal CycE transcription	0.41	0.01-1, Log
ν_{Ec}	Cooperativity of E2F1 on CycE transcription	7	1-8, Integer
κ_{Rc}	E2F1/Rbf dimer half maximal inhibition of CycE transcription	0.087	0.01-1, Log
ν_{Rc}	Cooperativity of E2F1/Rbf dimer on CycE transcription inhibition	1	1-8, Integer
Δt_C	Delay in CycE transcription & translation	15	1-5, Log
	GEM regulation:		
r_{Ag}	Maximal rate of APC^{fzr} degradation of Gem	0.22	$0.1L_g$ -$10L_g$, Log
κ_{Ag}	APC^{fzr} half maximal degradation of Gem	0.28	0.01-1, Log
ν_{Ag}	Cooperativity of APC^{fzr} degradation of Gem	7	1-8, Integer
	APC^{fzr} **regulation:**		
r_A	Rate of spontaneous APC^{fzr} activation	0.016	0.005-1, Log
r_{Ca}	Maximal rate of APC^{fzr} inactivation by CycE	646	$1/r_A$ -$25/r_A$, Log
κ_{Ca}	CycE half maximal inactivation of APC^{fzr}	0.74	$0.2\kappa_{Cs}$ -$1.5\kappa_{Cs}$, Log
ν_{Ca}	Cooperativity of CycE on APC^{fzr} inactivation	4	1-8, Integer
	DNA licensing & S-phase:		
K_{UD}	Rate of Dup binding to U	0.12	0.005-1, Log
r_{Cs}	Maximal rate of PreRC firing (S-phase initiation) by CycE	0.063	0.005-1, Log
κ_{Cs}	Half maximal CycE for triggering S-phase	0.065	0.01-1, Log
ν_{Cs}	Cooperativity of CycE on triggering S-phase	3	1-8, Integer
Δt_S	Time delay between PreRC firing and completion of S-phase (return to U)	40	20-50, Linear
	$CRL4^{Cdt2}$ **regulation & activity:**		
κ_{CULe}	Half maximal $CRL4^{Cdt2}$ for destroying E2F1	0.068	0.01-1, Log
ν_{CULe}	Cooperativity of $CRL4^{Cdt2}$ on destroying E2F1	5	1-8, Integer
r_{CULe}	Maximal rate of E2F1 degradation by Cul4 activity	0.29	$5L_e$ -$25L_e$, Log

κ_{CULd}	Half maximal CRL4^{Cdt2} for destroying Dup	0.11	0.01-1, Log
ν_{CULd}	Cooperativity of CRL4^{Cdt2} on destroying Dup	1	1-8, Integer
r_{CULd}	Maximal rate of Dup degradation by CRL4^{Cdt2} activity	0.72	$5L_d$ -$25L_d$, Log
κ_{Scul}	Half maximal S for activating CRL4^{Cdt2}	0.11	0.01-1, Log
ν_{Scul}	Cooperativity of S on activating CRL4^{Cdt2}	7	1-8, Integer
r_{Scul}	Maximal rate of CRL4^{Cdt2} activation by S-phase	0.08	0.005-1, Log
H_{CUL}	Mean lifetime of active CRL4^{Cdt2}	10.4	5-200, Log
	Regulation of Rbf:		
κ_{Cr}	CycE concentration for half maximal Rbf phosphorylation	0.011	0.01-1, Log
ν_{Cr}	Cooperativity of CycE on Rbf phosphorylation	5	1-8, Integer
r_{Cr}	Rate of Rbf phosphorylation by CycE	0.050	0.01-2, Log
r_{Dr}	Rate of Rbf dephosphorylation	0.074	0.01-1, Log
	Dimerization & cleavage rates:		
K_{RE}	Rate of E2F1 Rbf dimerization	0.01	0.005-1, Log
K_{ER}	Rate of E2F1/Rbf dimer dissociation	0.076	0.005-1, Log
K_{ERp}	Rate of E2F1/Rbf p dimer dissociation	0.75	$10K_{ER}$ -$100K_{ER}$, Log
K_{GD}	Rate of Gem Dup dimerization	2.68	$5K_{UD}$ -$25K_{UD}$, Log
K_{DG}	Rate of Gem/Dup dimer dissociation	0.026	$0.01K_{GD}$ -$0.1K_{GD}$, Log
	Mean Lifetimes of mRNA & proteins:		
H_E	Mean lifetime of E2F1	49.6	5-200, Log
H_R	Mean lifetime of Rbf	47.6	5-200, Log
H_c	Mean lifetime of CycE mRNA	15.7	5-100, Log
H_C	Mean lifetime of CycE	15.6	5-200, Log
H_G	Mean lifetime of Gem	122	5-200, Log
H_D	Mean lifetime of Dup	72.9	5-200, Log
	Transcription & translation rates:		
L_e	E2F1 synthesis rate	0.02	$1/H_E$, Fixed
L_r	Rbf synthesis rate	0.13	$0.05/H_R$-$20/H_R$, Log
C_c	CycE transcription rate	0.06	$1/H_c$, Fixed
C_{Cc}	Basal CycE transcription in absence of E2F1 activation	0.014	0.01-0.2
L_c	CycE translation rate	0.06	$1/H_C$, Fixed
L_g	Gem synthesis rate	0.027	$0.1/H_G$ -$100/H_G$, Log
L_d	Dup synthesis rate	0.090	$0.1/H_D$ -$10/H_D$,Log

Table S2: Fraction of lifelike parameter sets that satisfy perturbation

Perturbation	Model perturbation	Required effect[Reference]	% of WT parameter sets satisfying criteria
E2F1 overexpression	Increase E2F1 synthesis (L_e x 3)	Cycle faster[Fig 2]	16%
Rbf loss of function	Eliminate Rbf protein ($L_r = 0$)	Cycle continues[24]	93%
Rbf overexpression	Increase Rbf synthesis (L_r x 10)	Arrest with high E2F1 and low CycE	50%
CycE overexpression	Add constitutively produced CycE	Arrest with high CycE, GEM, and E2F1[Fig 2]	2%
Ago loss of function	Increase CycE protein stability (H_C x 10)	Slow/arrest with high CycE[Fig S1]	25%
Dap overexpression	Eliminate CycE protein activity ($r_{Cr} = 0$, $r_{Cs} = 0$, $r_{Ca} = 0$)	Arrest with high E2F1[Fig2]	100%
Starvation slow	Decrease all translation by 33% (E2F1, Rbf, Gem, Dup and CycE) (All L x 0.67)	Cycle slows, hypothesized as a way to regulate period[21,22]	46%
Starvation arrest	Decrease all translation by 80% (E2F1, Rbf, Gem, Dup and CycE) (All L x 0.2)	Arrest with low E2F1 and CycE[Fig 4]	83%
Dp loss of function	Eliminate E2F1 protein ($L_e = 0$)	Cycle slows but does not completely arrest[Fig 2]	4%
$E2F1^{PIP3A}$	Add E2F1 that cannot be degraded by $CRL4^{Cdt2}$ activity ($L_{ep} = 2\ L_e$)	Arrest with high E2F1 and high CycE[Fig 2, Fig 3]	99%
Loss of $CRL4^{Cdt2}$	No $CRL4^{Cdt2}$ activity ($r_{CULe} = 0$, $r_{CULd} = 0$)	Arrest with high E2F1 and high CycE	100%
Loss of APC^{fzr} function	Elimination of APC^{fzr} degradation of Gem ($r_{Ag} = 0$)	Cycle slows/arrests with high E2F1 and CycE activity[20]	6%
Gem overexpression	Add constitutively produced Gem (L_g x 10)	Cycle slows/arrests with high E2F1 and CycE[20]	10%
All of above	The parameter set reproduces the effect of each perturbation above		0.004 %

5. Supplementary Figures

Figure S1: SCF/Ago-mediated degradation is essential for endocycle progression

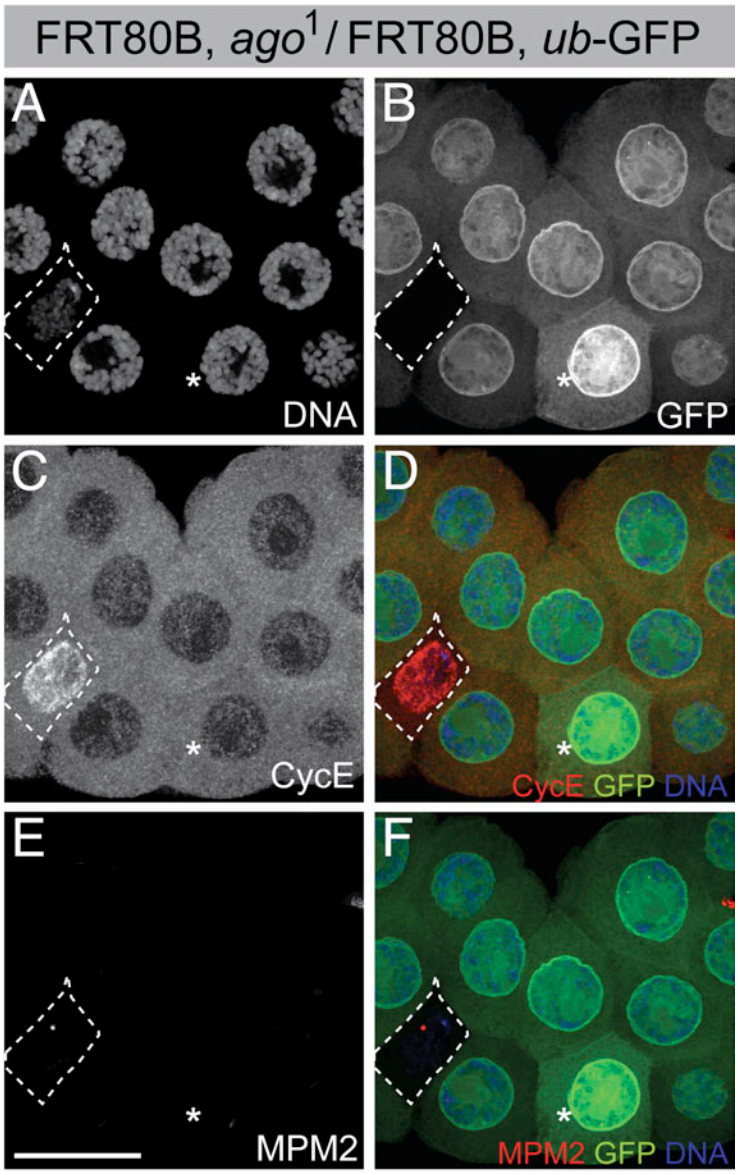

Figure S1: L3 salivary gland (96-104h AED) containing a cell mutant for the F-Box protein *archipelago* (cell enclosed in dotted line). *Ago*^{1} mutant cells were generated by mitotic recombination and were marked by the absence of GFP expression. The asterisk indicates the twin-clone containing two copies of the *ub*-GFP construct. **A)** DNA staining reveals that *ago*^{1} mutant cells have smaller nuclei than the adjacent control cells, indicating that the SCF^{Ago} complex is essential for endocycle progression in salivary glands. **C-D)** By this time (96-104h AED), salivary gland cells have exited the endocycle and have no Cyclin E protein. However, Cyclin E protein persists in *ago*^{1} mutant cells, demonstrating that the SCF^{Ago} complex is essential for Cyclin E degradation in larval salivary glands. **E-F)** *Ago*^{1} mutant cells display MPM-2 positive nuclear spheres, which are characteristic for cells with high levels of CDK activity. Scalebar: 50µm.

Figure S2: *dacapo* mutant salivary glands can endocycle normally

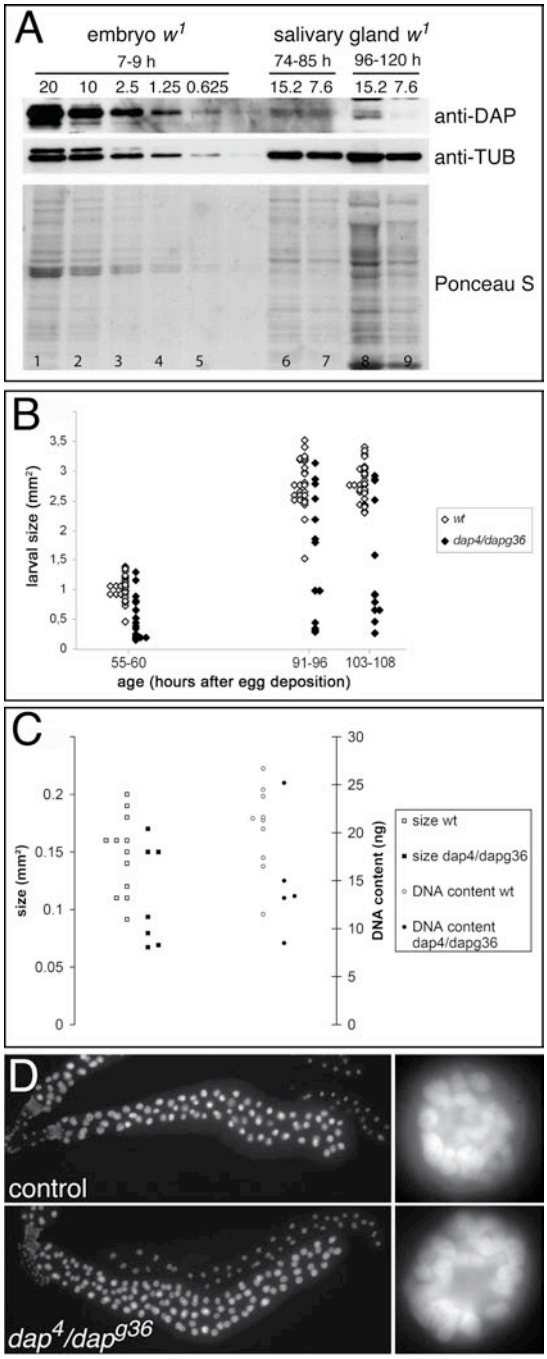

Figure S1: **A)** Dap protein levels are reduced in larval salivary glands. Extracts from embryos and salivary glands of indicated time after egg deposition were analyzed by Western blotting using antibodies against Dap and Tubulin. Ponceau S staining shows total protein levels. The number of embryos or salivary glands per lane is indicated. Lanes 2, 7, and 9 show similar staining for tubulin and Ponceau S. In larval salivary glands (lines 7 and 9), however, only trace amounts of Dap protein are present. **B-D)** dap^4/dap^{g36} mutant larva had ~7% viability to the wandering L3 stage (103-108 hrs AED) and most showed a 10-20 hr delay in pupariation (data not shown). **B)** Although a significant fraction of dap^4/dap^{g36} mutant larvae were smaller than controls ($dap^4/CyO,Act\text{-}GFP$ or $dap^{g36}/CyO,\ Act\text{-}GFP$) at all larval stages, some dap^4/dap^{g36} mutants were normal size, consistent with normal rates of endocycle progression in many larval tissues. **C)** At the L3 wandering stage, the size (squares) and DNA content (circles) of salivary glands from dap^4/dap^{g36} fell within the same range as heterozygous controls, though the average gland size and DNA content were reduced. **D)** DNA staining showing examples of salivary glands (left), and close-up of single nucleus (right), from a control $dap^{g36}/CyO,\ Act\text{-}GFP$ and a dap^4/dap^{g36} mutant at the wandering L3 stage (103-108 hrs AED). A likely cause of the growth delay in *dap* mutants are defects in the nervous system that affect feeding or systemic metabolism. The variable effects seen in the salivary glands could be secondary and non-cell autonomous.

Figure S3: Phasing of CycE, Gem, and E2F1

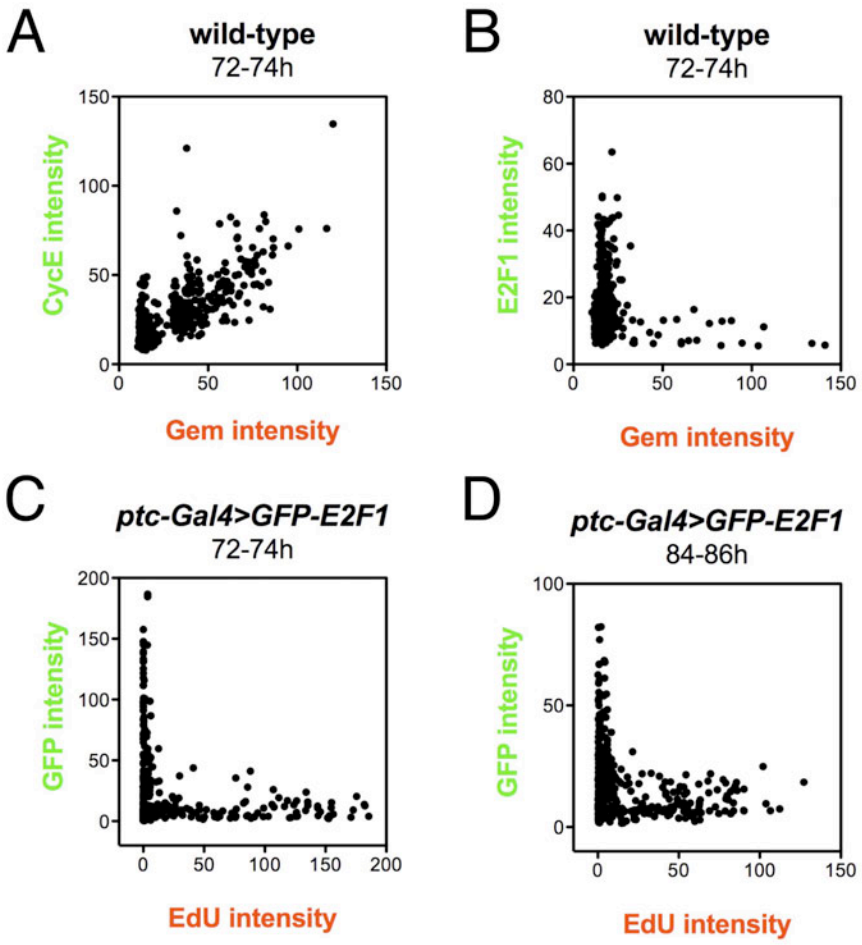

Figure S3: Graphs showing nuclear concentrations of E2F1, Gem, CycE and the S-phase marker EdU measured from micrographs of 5-8 salivary glands, in which each dot represents one nucleus. **A)** Consistent with the idea that Gem accumulation relies on CycE-dependent APC inhibition, we found significant overlap between CycE and Gem stainings at 72-74h AED. **B)** E2F1 and Gem signals were mutually exclusive at 72-74h AED, supporting the model that E2F1 protein disappears in S-phase. **C-D)** GFP-E2F1 overexpressed under control of the *ptc*-Gal4 showed a cell cycle distribution similar to endogenous E2F1 B). At 84-86h AED a fraction of S-phase cells (EdU-positive) with persisting GFP signal was noticeable. These cells presumably represent cells in which the level of GFP-E2F1 exceeded the capacity of the $CRL4^{Cdt2}$ ubiquitin ligase and that will eventually arrest the endocycle.

Figure S4: Full schematic of endocycle network

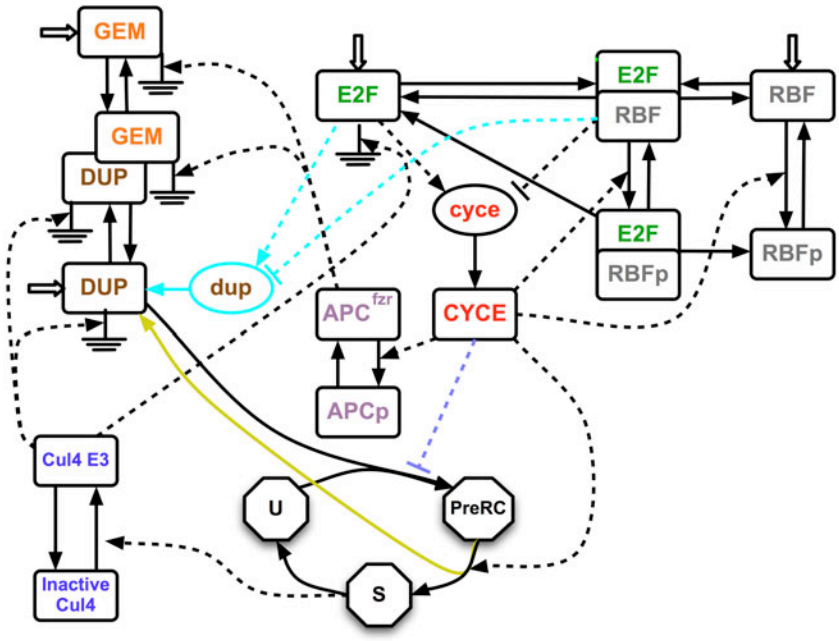

Figure S4: Schematic of the full endocycle network showing the regulatory interactions and biomolecules in our model. mRNAs are indicated by lowercase ovals, proteins by uppercase squares, the state of the replication complex(licensing) by octagons, and heterodimers by connected squares. Solid lines indicate fluxes with the arrow pointing towards the product, dashed lines are regulatory interactions, activators end in arrowheads, inhibitors end in bars, large arrows indicate constitutive production, ground symbols indicate regulated degradation. Black lines show interactions in the standard model; we also explored the effects of alternate regulatory interactions shown with colored lines and shapes. APC^{fzr} and $CLR4^{Cdt2}$ transition between active and inactive forms. All mRNA and proteins (except APC and $CLR4^{Cdt2}$) decay independently with 1st order kinetics.

Figure S5: Implementation of time delays

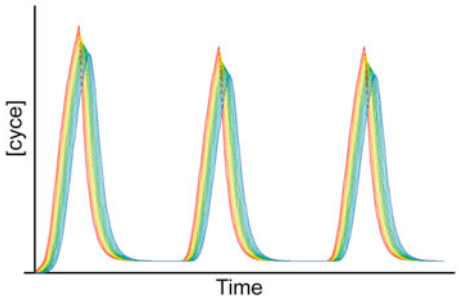

Figure S5: Time delays were implemented as a long series of sequential processes that produce an effective time delay with mild lowpass filtering. Plot shows an example of time delayed CycE mRNA concentration. Red line indicates non-delayed trajectory, with successive colors (cycling from red to blue) showing increasingly delayed versions

calculated according to Equation 3. We chose a cascade of N = 10, as this balanced computation speed with little attenuation of the non-delayed waveform.

Figure S6: Histograms of parameter values enabling lifelike oscillations in model

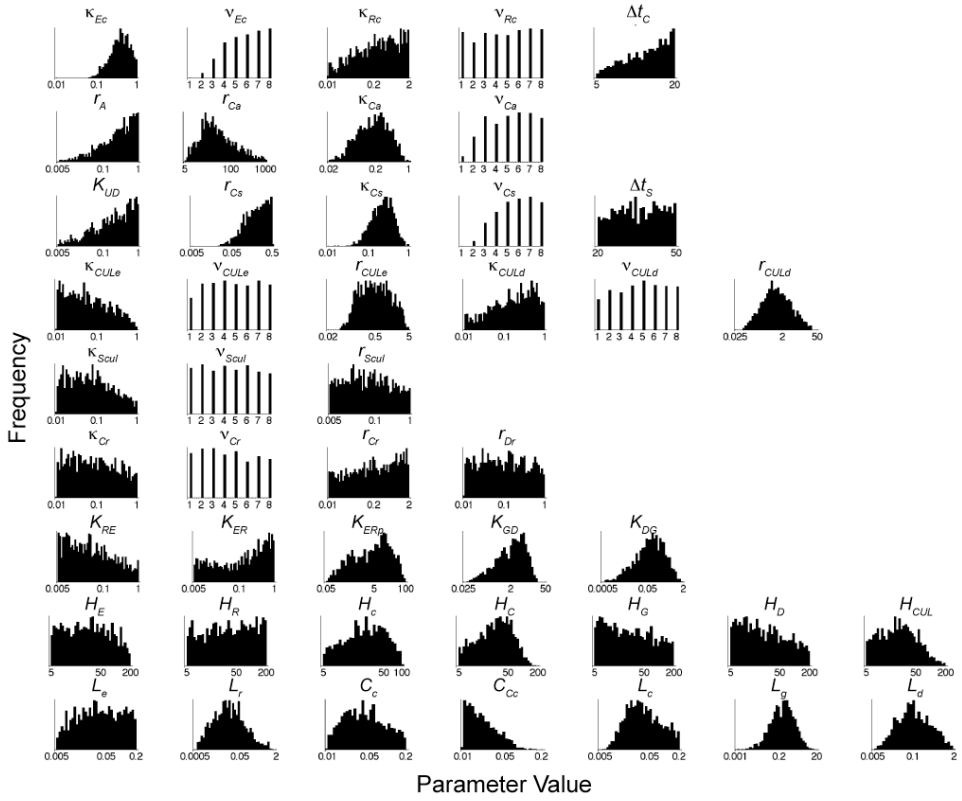

Figure S6: Histograms of parameter values (n = 1375) that enabled lifelike oscillations (i.e. that reproduced our measurements of wild type cycles). Horizontal axes are plotted on a log scale (except those for cooperativities), and the vertical axis represents the relative frequency of each parameter value plotted on a linear scale. For some parameters only a limited range of values produced wild type oscillations in our model. All parameters are defined with sampled ranges in Table S1.

Figure S7: Cross Correlations between parameters

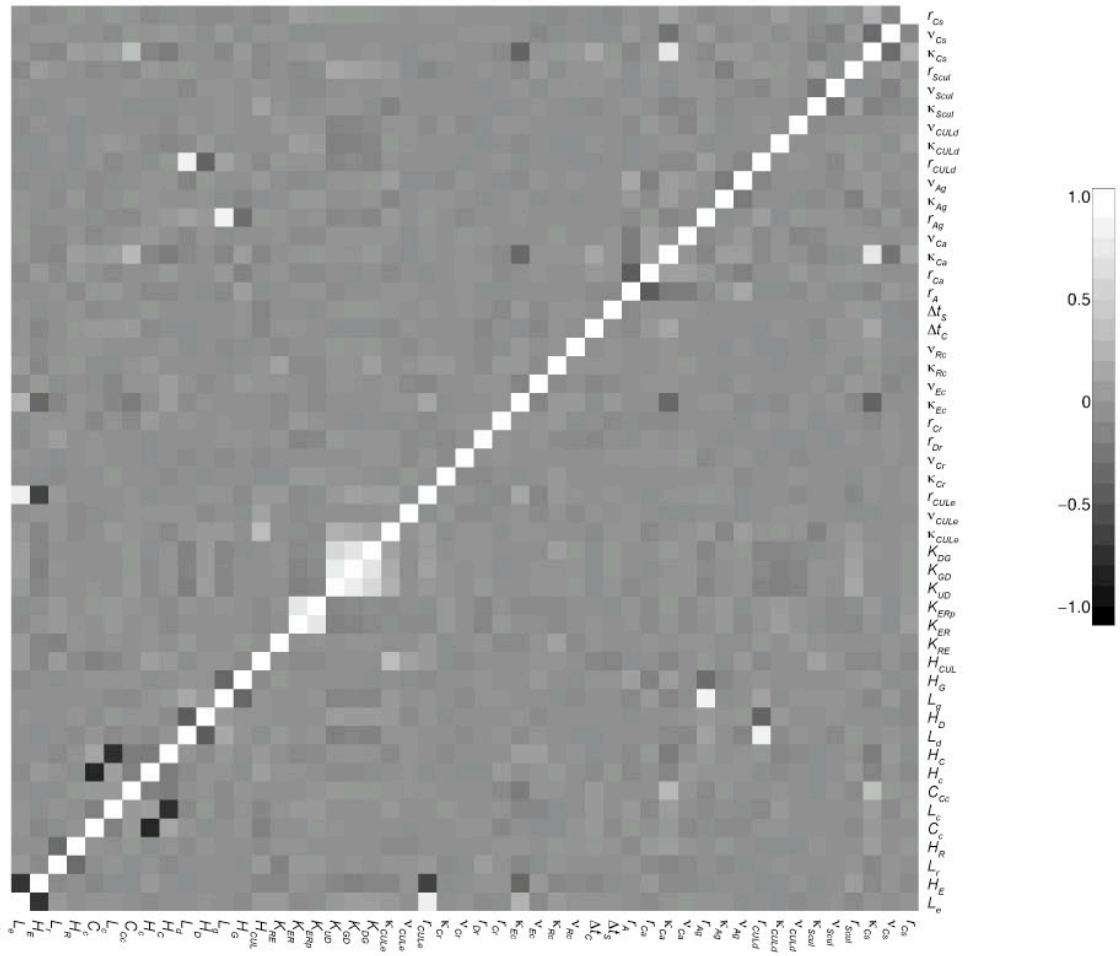

Figure S7: Pairwise cross correlation coefficients in 1375 parameter sets producing wild type oscillations. A cross correlation coefficient of 1 (white) indicates complete correlation, -1 indicates complete anticorrelation (black), and 0 is uncorrelated. Elements along the main diagonal correlate with themselves and thus have a value of 1. All of the strong correlations were due to restrictions on the parameters imposed during the random search as described in Table S1. Most correlation coefficients were close to 0 indicating that compensation, if present, involved groups of 3 or more parameters.

Figure S8: Effect of parameters on cycle period

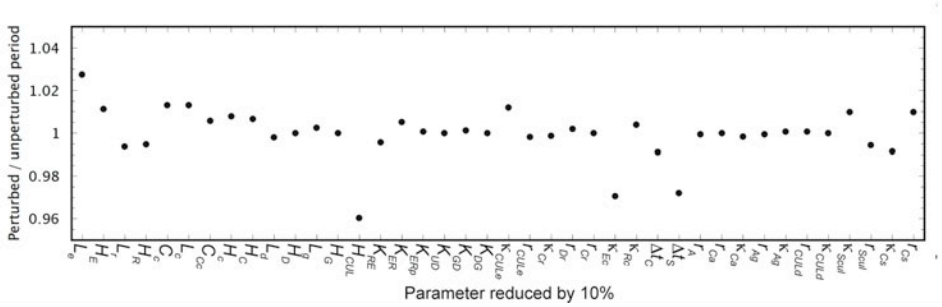

Figure S8: The effect of reducing each parameter on the period of oscillation. We perturbed 12 parameter sets producing wild-type oscillations and all criteria in Table S2. For each of the parameters, we reduced its value by 10% while keeping all others unchanged, and calculated the ratio of the new period to the original period. Results were averaged across all parameter sets. A value of 1 indicates no net change in period, greater than 1 indicates the period increases as the parameter is reduced, less than 1 indicates period decreases as the parameter is reduced.

Figure S9: Robustness to parameter perturbation.

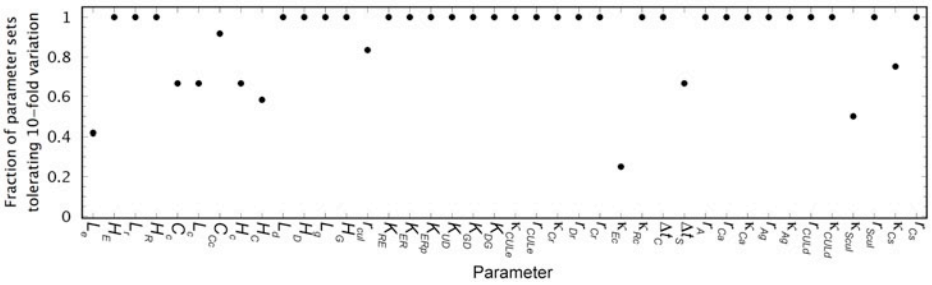

Figure S9: The endocycle network produces oscillations that are robust to changes in single parameters. Starting with the 12-parameter sets that reproduce wild-type oscillations and all the phenotypes of all perturbations in Table S2, we varied each of the parameters over 2 orders of magnitude in 8 steps. The fraction of parameter sets that could be varied by at least an order of magnitude (10-fold change) and continue cycling is plotted on the Y-axis (1 = 10-fold change always tolerated, 0 = 10-fold change never tolerated).

Figure S10: Endocycle model reproduces experimental perturbations

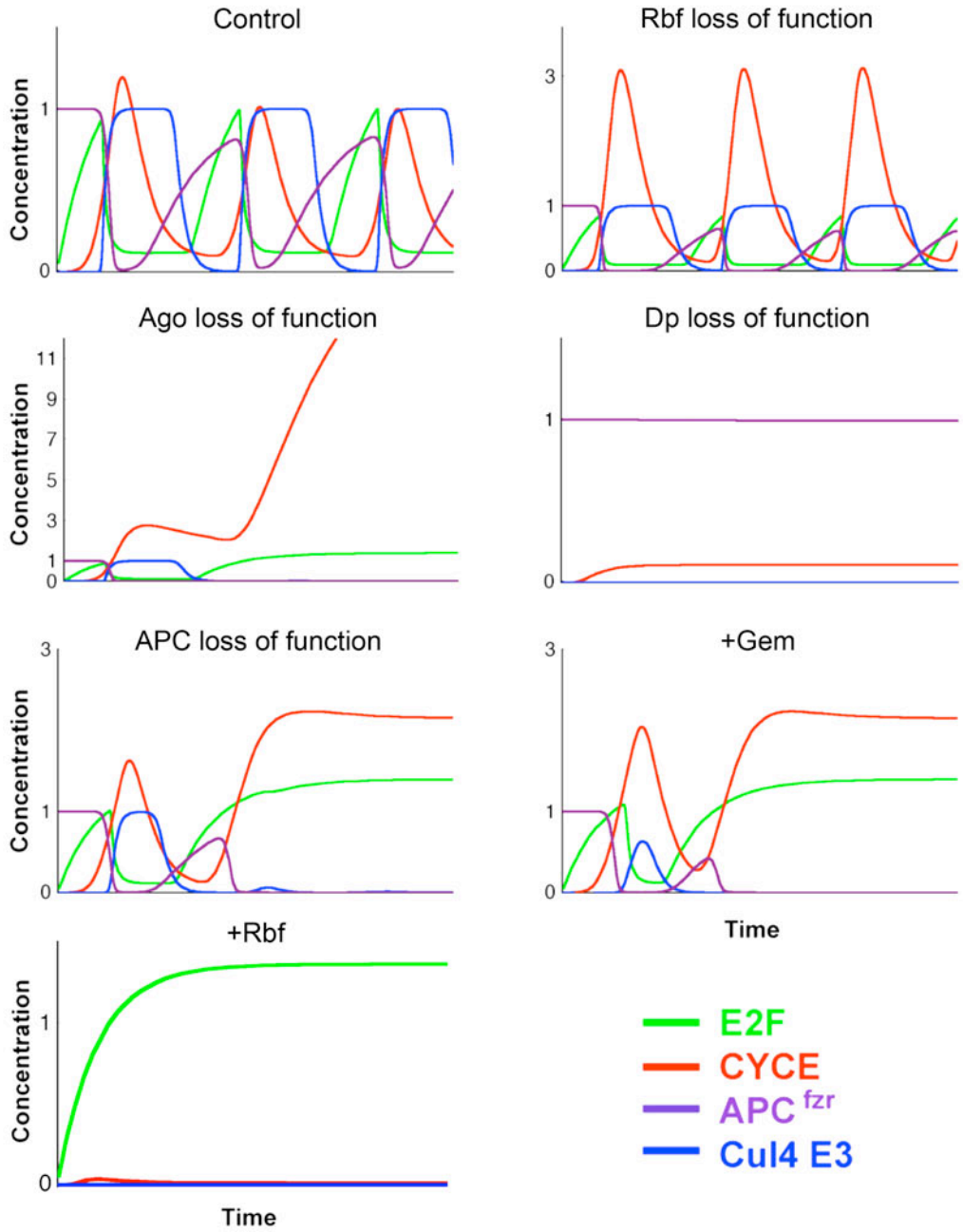

Figure S10: All panels show the same parameter set showing the effect of perturbations in Table S2. The E2F1 line shows the concentration of all forms of E2F1/Dp (sum of all free E2F1, E2F1 bound to Rbf, and $E2F1^{PIP3A}$). All concentrations are normalized to their maximal value during steady state oscillation during wild-type (control) cycling. Note different vertical axes ranges between plots; horizontal (time) axis is constant for all plots.

Figure S11: Endocycle arrest by E2F1 stabilization

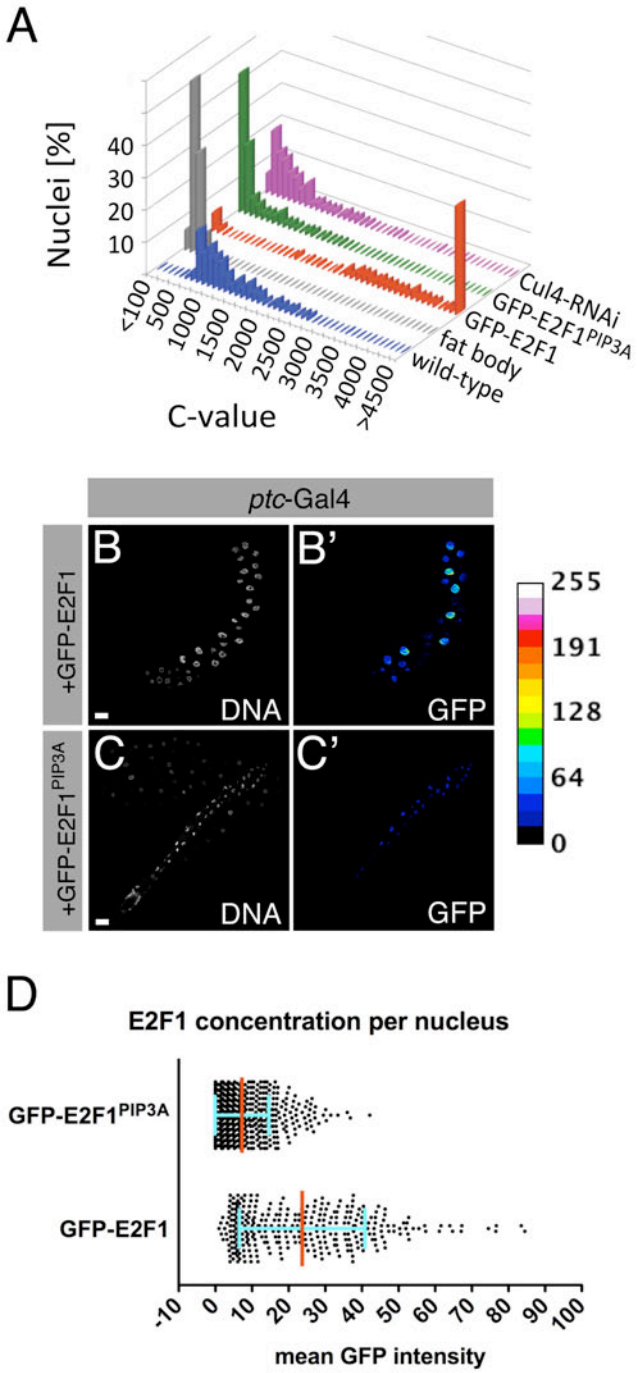

Figure S11: **A)** C-values of individual nuclei in the indicated genotypes of salivary glands, measured at 96-98h AED. Overexpression of GFP-E2F1 led to higher C-values than measured in wild-type salivary glands, while overexpression of GFP-E2F1^{PIP3A} or Cul4-RNAi resulted in significantly lower DNA contents. **B-C)** Matched exposure images of GFP-E2F1 (B) and GFP-E2F1^{PIP3A} (C) in salivary glands at 96-98h AED as used for fluorescence intensity measurements, shown as an intensity heat-map. **D)** GFP fluorescence intensity measurements displayed as mean pixel intensity/nucleus as shown

in B and C, assayed by confocal microscopy with Avalanche Photodiode Detectors. Each dot represents the mean GFP intensity/pixel for one nucleus. 324 nuclei from 5 glands were measured for GFP-E2F1, and 577 nuclei from 6 glands were measured for GFP-E2F1^{PIP3A}, both at 96-98h AED. GFP-E2F1 (B') was expressed at higher levels than GFP-E2F1^{PIP3A} (C') with mean GFP intensities of 23.69 vs. 7.26. See methods for further details of the measurement technique.

Figure S12: Endocycle arrest by Cul4-RNAi

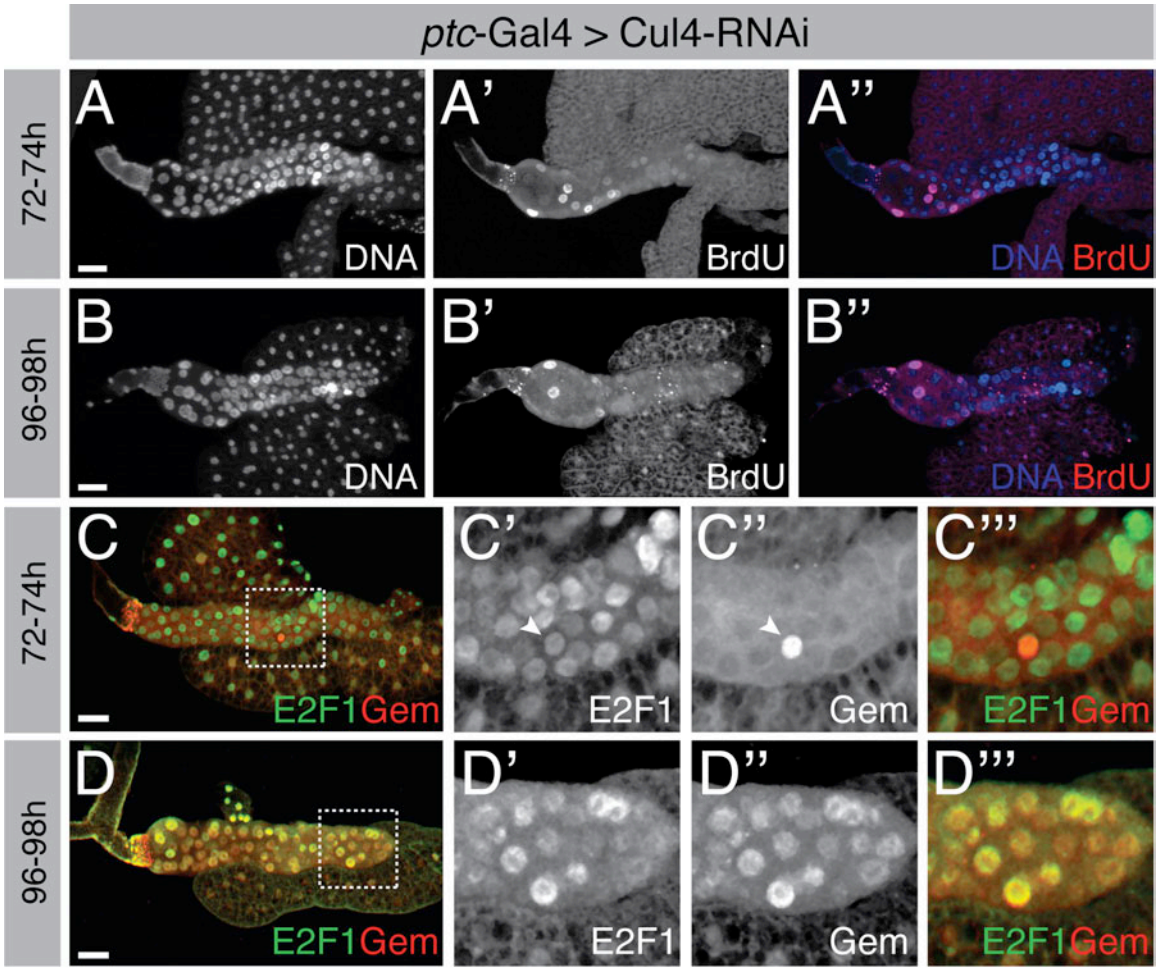

Figure S12: *ptc*-Gal4-mediated overexpexpression of Cul4-RNAi. Salivary glands were analyzed at 72-74h and 96-98h AED. Scale bars = 50µm. **A-B)** Cul4-RNAi suppressed DNA replication, indicated by diminished BrdU incorporation (A', B') and no noticeable accumulation of mass between both time points. **C-D)** Cul4-RNAi caused accumulation of E2F1 at early and late time points (C', D'), while Geminin was only observed at late time points (C", D"). The delay between E2F1 stabilization and appearance of Geminin, suggests that the accumulation of Geminin is rather a consequence than the actual cause of endocycle arrest. Dashed lines indicate the regions shown in the close-ups in C and D.

Figure S13: E2F1 is essential for endocycle progression

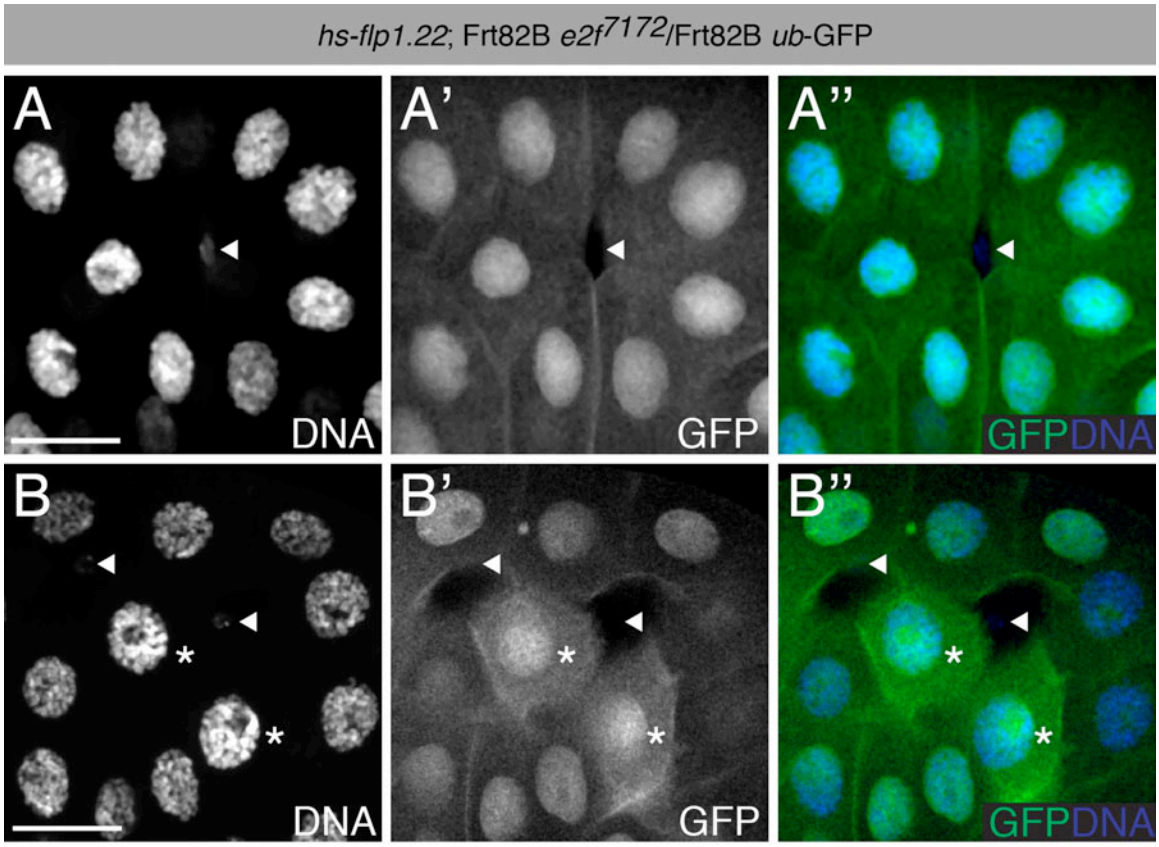

Figure S13: **A-B)** Two examples of mosaic salivary glands containing *e2f*^{7172} mutant cells. Mitotic recombination was induced in the salivary placode at 2-4h AED. Salivary glands were dissected 96-98h AED and subsequently stained with DAPI (blue) to visualize DNA contents. Scale bars = 50µm. Cells heterozygous for *e2f*^{7172} express one copy of GFP (green). Cells homozygous for the *e2f*^{7172} allele were marked by absence of GFP (arrow heads), while the corresponding wild-type sister clones were labeled with two copies of GFP (asterisks). Loss of E2F1 resulted in small cells with vastely reduced DNA contents compared to the neighboring control cells (see also Fig 2B). Consistent with E2F1's proposed function as a pacemaker of the endocycle, *e2f*^{7172} heterozygous cells had about half the DNA content of wild-type *(e2f*$^{+/+}$*)* cells (B).

Figure S14: Endocycle progression is delayed in *Dp* mutants

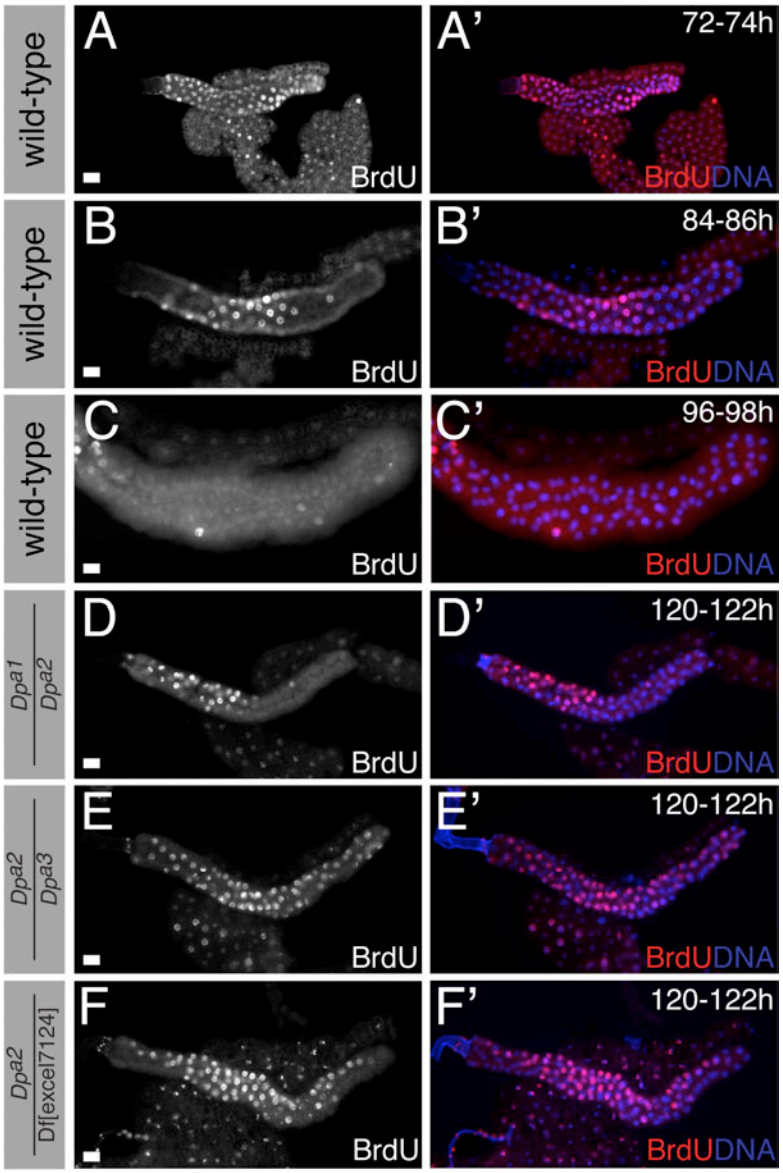

Figure S14: Photomicrographs showing endocycle progression in wild-type and *Dp* mutant salivary glands. Salivary glands were dissected at the indicated time points (upper right corner) and labeled for 1h with BrdU to visualize ongoing DNA replication. Scale bars = 50µm. **A-C)** At 72-74h and 84-86h AED BrdU incorporation was readily detectable in a large fraction of cells, while at 96-98h AED most of the cells had exited the endocycle and were thus negative for BrdU staining. **D-F)** Micrographs of representative salivary glands of three different combinations of *Dp* alleles. From DNA sequence, Dp^{a2} and Dp^{a3} are believed to be null alleles, and Dp^{a1} is a strong hypomorph. Loss of *Dp* resulted in a severe delay of salivary gland growth. At 120-122h AED BrdU incorporation was readily detectable (D-F), while wild-type salivary glands have completed endoreplication at about 96-98h AED (C). Comparison of salivary gland sizes showed that at 120-122h AED salivary glands in *Dp* mutants (D-F) had only reached a stage corresponding to wild-type salivary glands at 84-86h AED.

Figure S15: *Dp* mutants show normal oscillation of E2F target genes

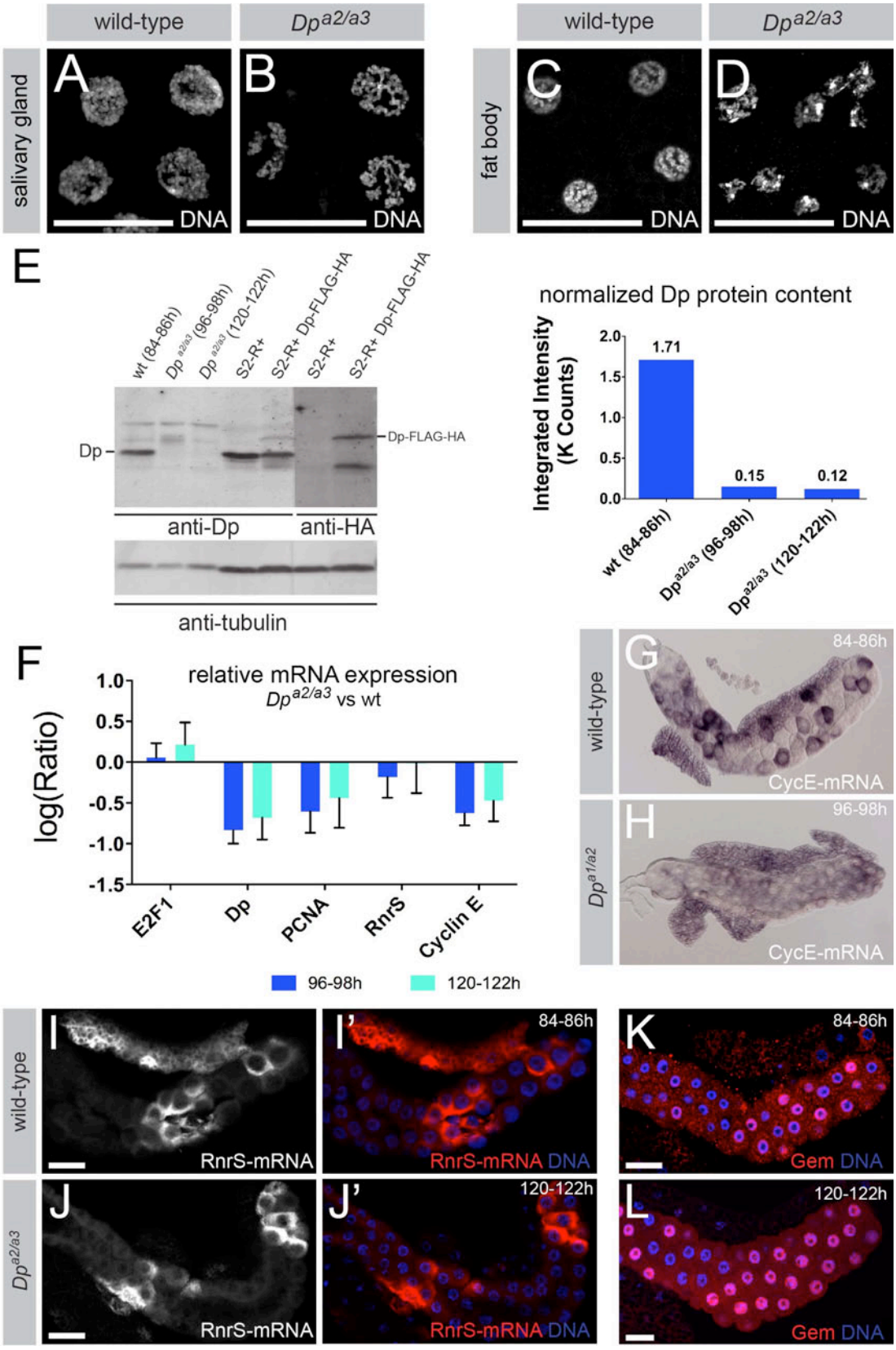

Figure S15: A-D) High magnification micrographs of nuclei from wild-type and $Dp^{a2/a3}$ mutants. To compensate for differences in developmental timing wild-type was analyzed at 84-86h AED, while $Dp^{a2/a3}$ mutants were aged to 120-122h AED. Scale bars represent 50µm. Loss of Dp resulted in aberrant chromosome morphology in the salivary gland (A-B) and the adjacent fat body (C-D). **E)** The western blot on the left side shows extracts derived from the following samples: lane #1: wild-type salivary glands 84-86h AED, lane #2: $Dp^{a2/a3}$ mutant salivary glands 96-98h AED, lane #3: $Dp^{a2/a3}$ mutant salivary glands 120-122h AED, lane #4: wild-type S2-R+ cells, lane #5: S2-R+ cells transfected with Dp-FLAG-HA, lane #6: wild-type S2-R+ cells, lane #7: S2-R+ cells transfected with Dp-FLAG-HA. Lanes #1-5 were probed with an anti-dDP antibody while lanes #6-7 were treated with an antibody against HA-tag. For normalization all lanes were also probed with an anti-tubulin antibody, which was detected in a separate channel. In wild-type (lane #1 & 4) a strong band was visible at around 50kD, which is the predicted size of Dp. In $Dp^{a2/a3}$ mutants (lane #2 & 3), however, only trace amounts of Dp protein were detectable. Ectopic expression of a FLAG-HA tagged Dp construct in S2-R+ led to an additional lower mobility band that was also detected with an antibody directed against the HA tag (Lane #7). Therefore, we conclude that the anti-Dp antibody specifically recognized Dp protein. The graph on the right shows the relative amounts of Dp protein normalized to the tubulin signal. This quantification revealed that $Dp^{a2/a3}$ mutant salivary glands still contained ~10% of the Dp protein that was detected in wild-type salivary glands. **F)** Relative expression analysis of E2F target genes mRNAs in $Dp^{a2/a3}$ mutants, as measured by RT-qPCR. Total mRNA from $Dp^{a2/a3}$ mutant salivary glands was isolated 96-98h and 120-122h AED. Both time points were compared to mRNA pools from 82-84h AED wild-type salivary glands. In the $Dp^{a2/a3}$ mutant levels of Dp transcripts were significantly reduced compared to wild-type, while the amount of E2F1 mRNA was unaffected. In addition, the expression levels of the E2F target genes *CycE, rnrS* and *pcna* were significantly reduced compared to wild-type. **G-H)** Spatial expression of CycE transcripts in wild-type and $Dp^{a1/a2}$ mutants analyzed by RNA *in situ* hybridization. In wild-type (84-86h AED) CycE was expressed in discrete domains (G)**.** In $Dp^{a1/a2}$ (84-86h AED) mutants CycE transcript was present at lower levels but the "oscillating" (on/off) pattern of CycE expression was similar to wild-type (H). **I-J)** Expression pattern of *rnrS* transcripts in wild-type (84-86h AED) and $Dp^{a2/a3}$ mutant salivary glands (120-122h AED). *rnrS* mRNA is shown in red, DNA staining (DAPI) in blue. Scale bars represent 50µm. In wild-type and in the $Dp^{a2/a3}$ mutant *rnrS* was only detectable in a subset of cells, demonstrating that this allelic combination does not prevent oscillation of this E2F target gene. **K-L)** Geminin protein oscillation in wild-type (84-86h AED) and $Dp^{a2/a3}$ mutant salivary glands (120-122h AED). Geminin protein is shown in red, DNA staining (DAPI) in blue. Scale bars = 50µm. In wild-type and in the $Dp^{a2/a3}$ mutants Geminin protein was only visible in a fraction of cells. Since accumulation of Geminin protein requires high levels of CycE/Cdk2 activity, this experiment further supports the idea that the $Dp^{a2/a3}$ mutant allows oscillation of E2F1 target genes.

Figure S16: Overexpression of stable E2F1 prevents endoreplication in *Dp* mutants

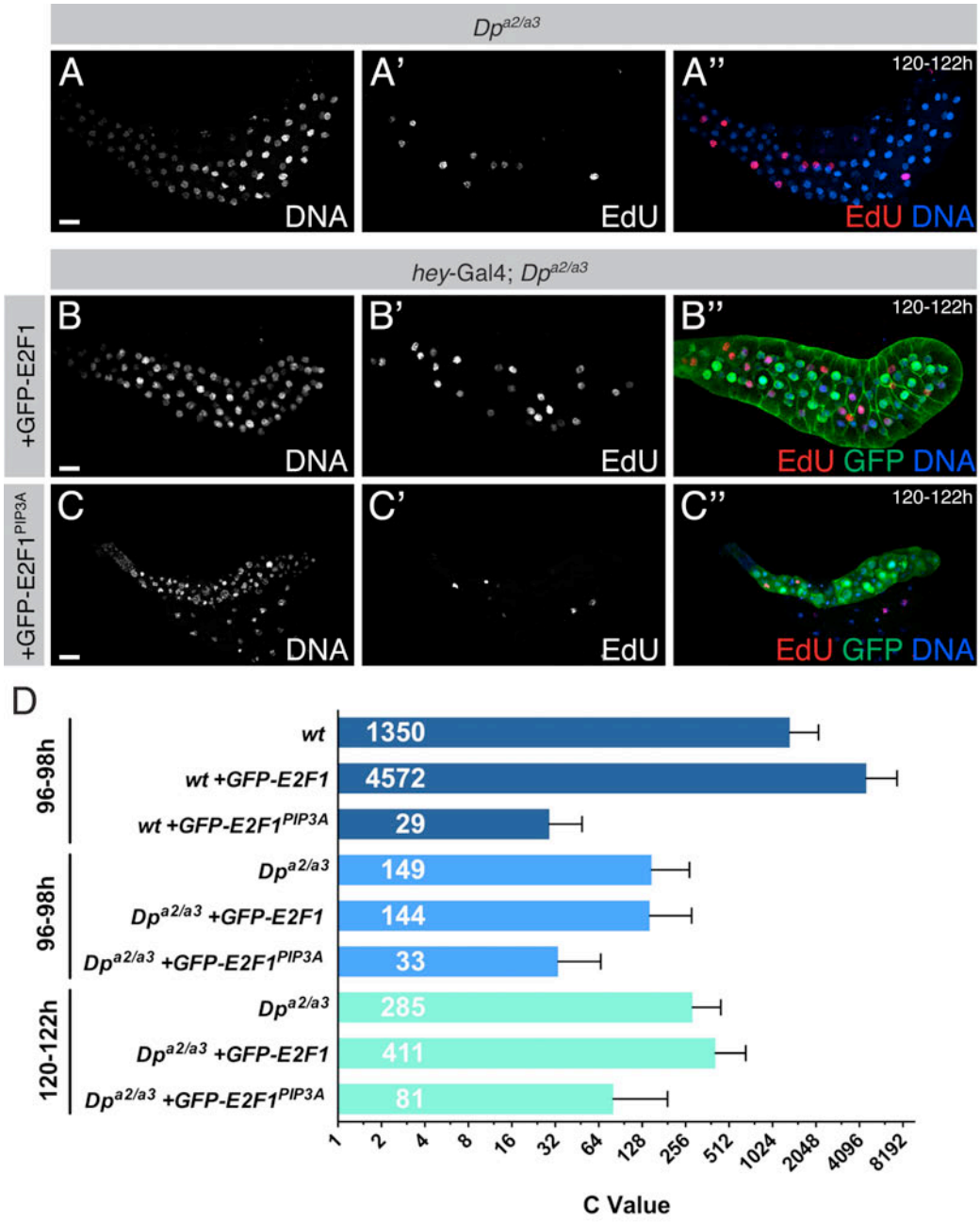

Figure S16: **A-C)** Salivary glands of the indicated genotypes were labeled for 1h with EdU at 96-98h AED. GFP-E2F1 fusion proteins were visualized by staining with a GFP antibody. *hey*-Gal4 was used for salivary gland-directed expression of UAS target genes in the $Dp^{a2/a3}$ mutant. Experiments were performed at 29˚C to allow maximal activation of the UAS constructs by Gal4. In the overlays in the right column EdU labeling is shown in red, GFP staining in green and DNA staining (DAPI) in blue Scale bars = 50µm. **A)** Despite being delayed in development, $Dp^{a2/a3}$ mutants showed a fairly normal pattern of DNA replication. **B)** S-phase progression in $Dp^{a2/a3}$ mutant salivary glands was not affected by overexpression of GFP-E2F1 (compare EdU labeling in A' and B'). **C)** Overexpression of stable E2F1 (GFP-$E2F1^{PIP3A}$) blocked endocycle progression in

$Dp^{a2/a3}$ mutant salivary glands as indicated by the absence of EdU incorporation (C'). Moreover, overexpression of non-degradable E2F1 caused severe defects in chromosome morphology C). **D)** Quantification of C-values per nucleus for the indicated genotypes and time points. Average C-values are listed within each bar. Overexpression of stable GFP-$E2F1^{PIP3A}$ in the $Dp^{a2/a3}$ background resulted in a dramatic decrease in nuclear DNA content compared to the $Dp^{a2/a3}$ mutant alone, while DNA content was only mildly increased upon overexpression of wild-type GFP-E2F1.

Figure S17: Geminin mutant cells endocycle

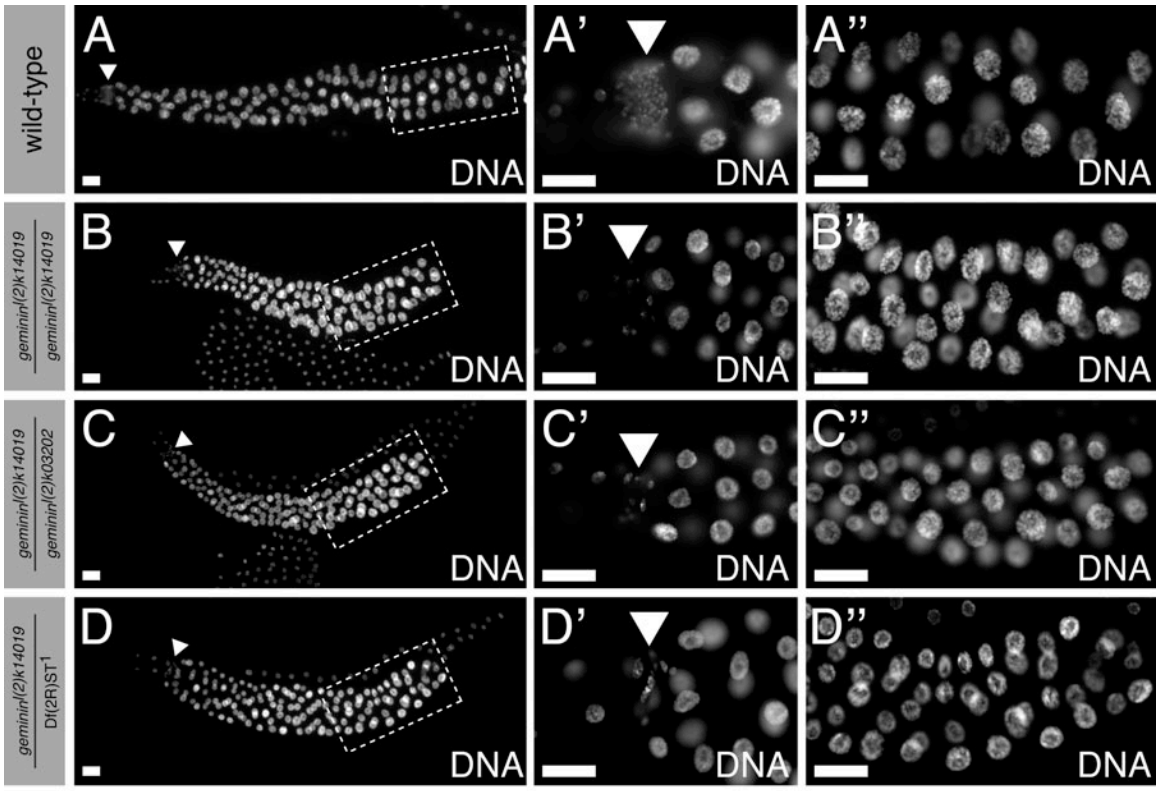

Figure S17: Micrographs showing representative salivary glands from wild-type animals (A) and three different combinations of *geminin* alleles, at 96-98h AED. Second column shows the imaginal ring (arrowheads), whose cells undergo mitotic division. Third column shows regions boxed in first the first column. Scale bars = 50µm. Average amount of DNA/nucleus is shown in Fig 3E. **A)** Wild-type salivary glands after completion of the endoreplication program. In wild-type, imaginal rings were comprised of ~200 cells. **B)** Salivary glands homozygous for the *gem* allele *l(2)k14019* are slightly reduced in size, but show normal DNA morphology (B''). The imaginal rings consist of only few cells with highly over-replicated DNA. **C)** Salivary glands heterozygous for the *gem* alleles *l(2)k14019* and *l(2)k03202* show normal DNA morphology, while the imaginal rings are over-replicated. **D)** Hemizygous animals carrying the *l(2)k14019* allele and the deficiency $Df(2R)ST^{1}$ showed a similar phenotype than animals homzygous for *l(2)k14019* (B), suggesting that *l(2)k14019* represents a null allele or at least a strong hypomorph. It is important to note that *gem* mutant amimals failed to devolop imaginal discs and thus the reduced size of the salivary glands is likely due to a delay in overal development.

Figure S18: Cyclin E but not Rca1 blocks endocycling in *gem* mutants

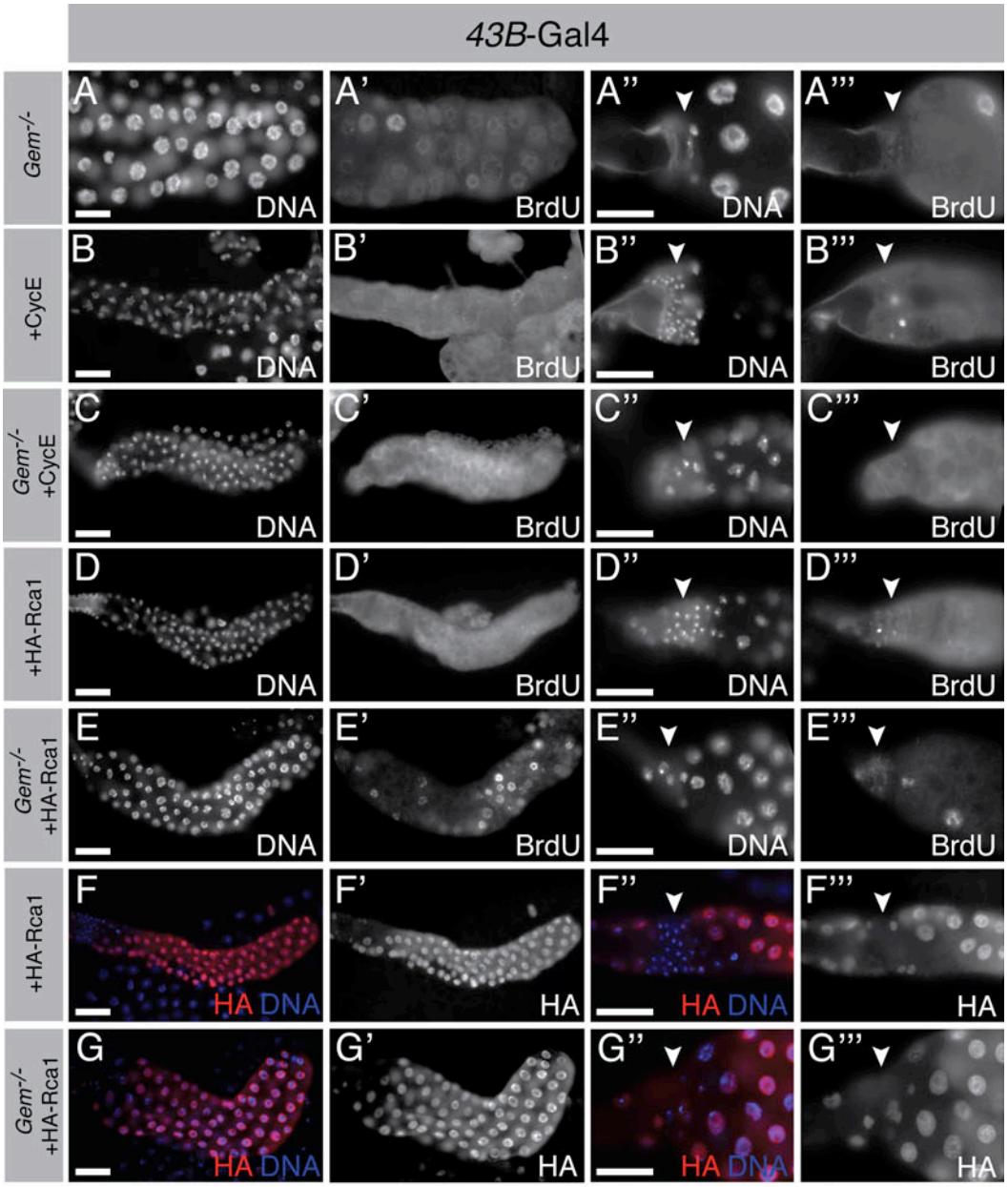

Figure S18: Salivary glands of the shown genotypes, stained as indicated, at 96-98h AED. 43B-Gal4 was used for salivary gland-directed expression of UAS target genes. Gem$^{-/-}$ indicates the *gemimin*$^{l(2)k14019}$/*gemimin*$^{l(2)k14019}$ genotype. Arrowheads in third and fourth columns (’’, ’’’) mark the mitotic imaginal ring, which is defective in *gem* mutants. Scale bars = 50µm. **A)** *Gem* mutants displayed normal DNA morphology and BrdU incorporation. **B-C)** Overexpression of CycE prevented S-phase in wild-type (B’) and *gem* mutant salivary glands (C’). **D-E)** Inhibition of APC activity by HA-Rca1 overexpression blocked endocycle progression in otherwise wt salivary glands (D’). S-phase inhibition by HA-Rca1 was suppressed in the *gem* mutant, as shown by BrdU incorporation (E’). **F-G)** Antibody staining against the HA epitope revealed that HA-Rca1 was expressed at comparable levels in wild-type and *gem* mutant salivary glands.

Figure S19: Loss of *Gem* does not rescue endocycle arrest caused by stable E2F1

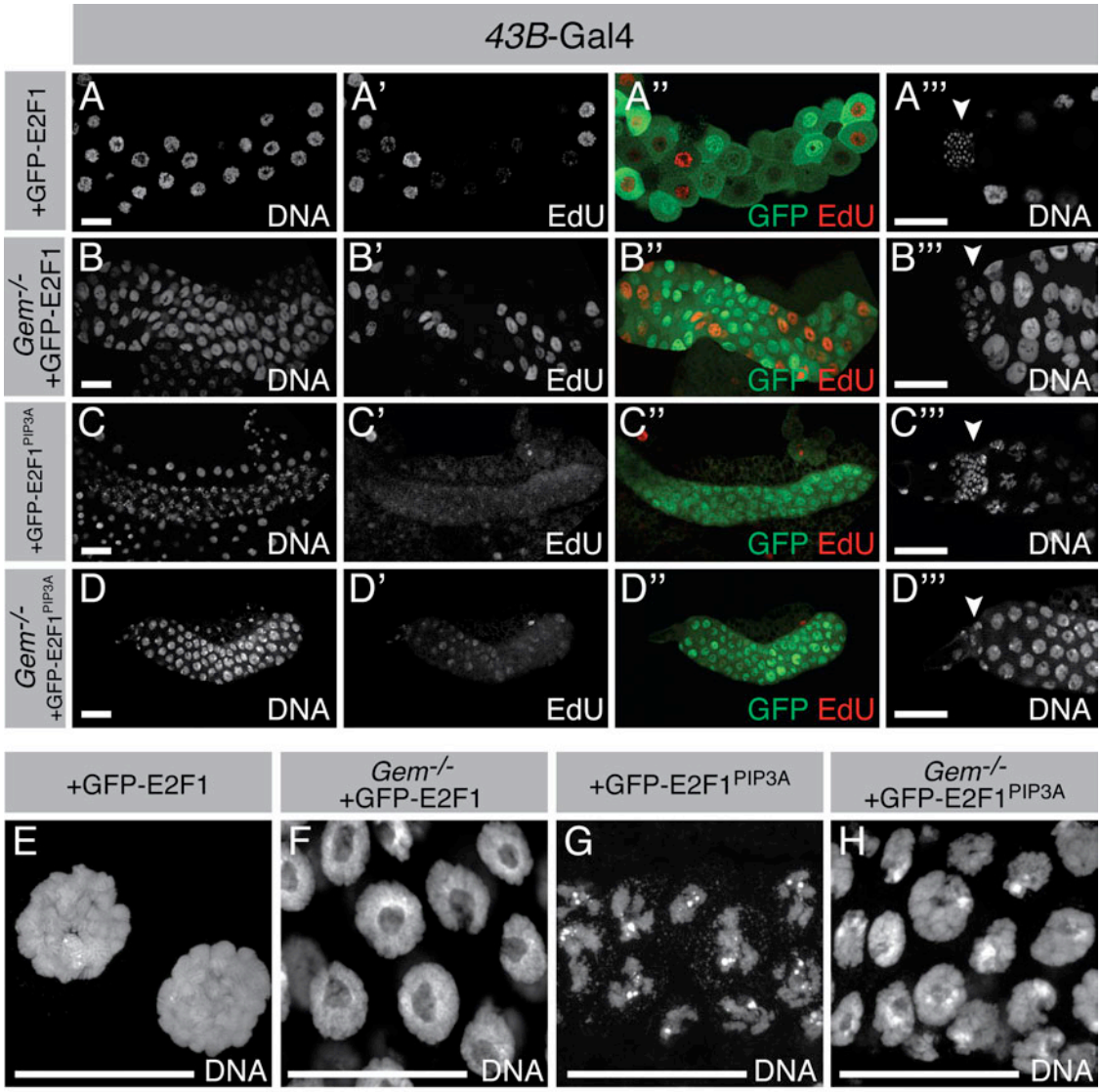

Figure S19: Salivary glands of the indicated genotypes, stained as noted, at 96-98h AED. 43B-Gal4 was used to drive salivary gland expression of the indicated UAS constructs. Gem$^{-/-}$ indicates the *gemimin*$^{l(2)k14019}$/ *gemimin*$^{l(2)k14019}$ genotype. Scale bars = 50µm**. A-B)** Overexpression of GFP-E2F1 allowed S-phase progression in wild-type (A') and *gem* mutant (B') salivary glands, as visualized by EdU labeling. **C-D)** Overexpression of stabilized E2F1 (GFP-E2F1^{PIP3A}) blocked nearly all EdU incorporation in both wild-type (C') and *gem* mutant (D') salivary glands. Arrowheads in the fourth column ('') mark the mitotic imaginal ring, which shows defective cell proliferation in *gem* mutants. **E-H)** Maximum projections of representative nuclei of the same genotypes as above. Scale bars = 50µm. **E-F)** Overexpression of GFP-E2F1 in wild-type or *gem* mutant salivary glands did not affect DNA morphology. **G)** Overexpression of GFP-E2F1^{PIP3A} caused severely disrupted nuclear morphology. **H)** Although loss of *gem* did not fully rescue the endocycle arrest caused by stabilized E2F1, a less aberrant DNA morphology was observed, demonstrating that ectopic accumulation of Geminin accounts for at least part of the phenotype.

Figure S20: Cyclin A and Cdk1 accumulation after E2F1 overexpression

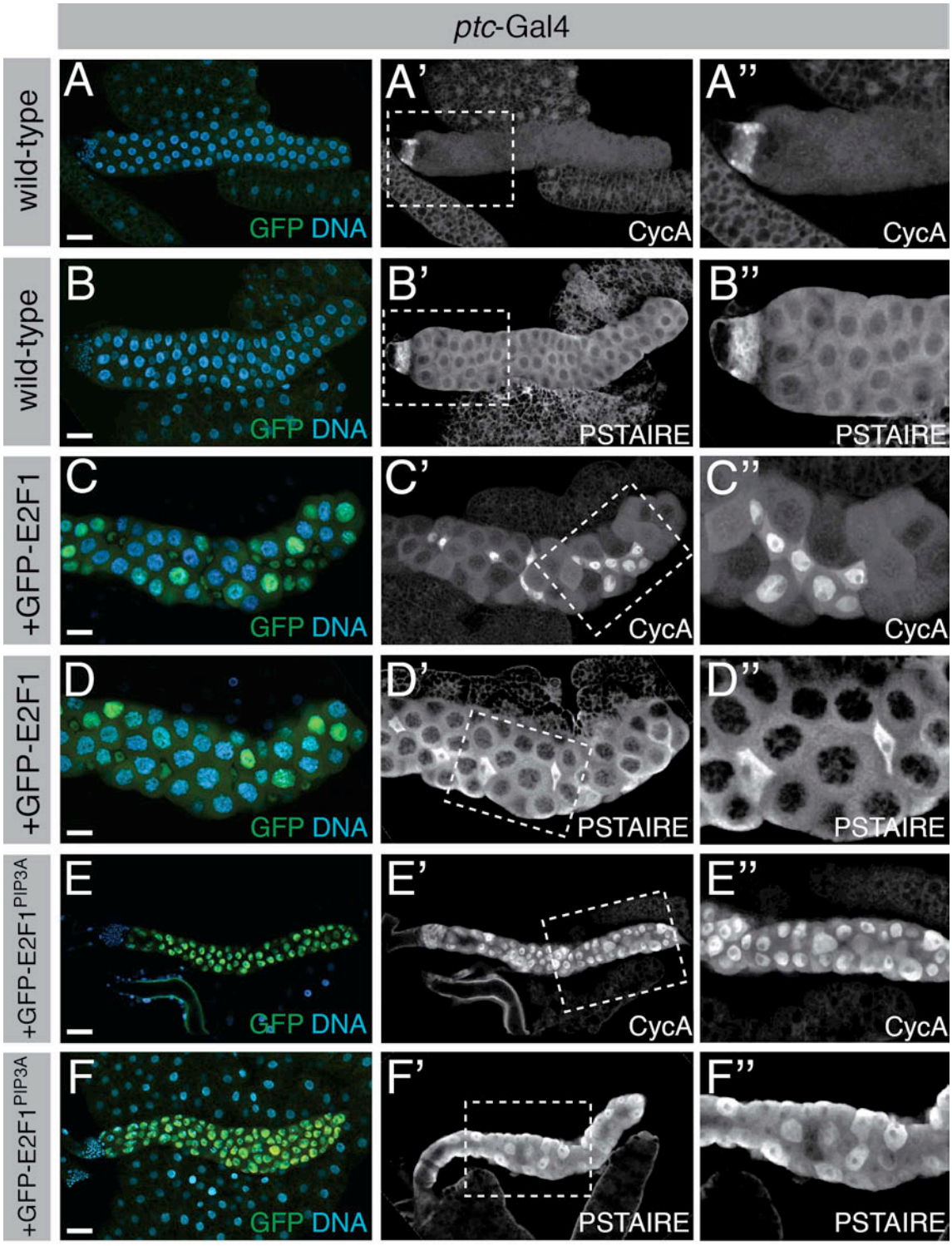

Figure S20: Wild-type (A-B) and E2F1 overexpressing salivary glands at 72-74h AED. First column shows GFP signals (green) from GFP-E2F1 (C-D) or GFP-E2F1^{PIP3A} (E-F) and DAPI (blue). Second column shows the levels of Cyclin A (A', C', E') or Cdk1 protein (B', D', F') detected with anti-PSTAIRE antibody. Third column (") shows regions boxed in second column ('). Scale bars = 50µm. **A-B)** In wild-type salivary

glands, a high levels of Cyclin A and Cdk1 were detected only in the mitotic imaginal ring cells, but absent in the endoreplicating cells of the salivary gland (A', A"). **C-D)** Upon ectopic expression of GFP-E2F1 Cyclin A as well as Cdk1 staining was visible in scattered cells throughout the salivary gland, whereby the signal was strongest in the small, arrested cells. **E-F)** Overexpression of GFP-E2F1^{PIP3A} led to high levels of Cyclin A and Cdk1 throughout the salivary gland.

6. Supplementary References

1 Moberg, K.H., Mukherjee, A., Veraksa, A., Artavanis-Tsakonas, S., & Hariharan, I.K., The Drosophila F box protein archipelago regulates dMyc protein levels in vivo. *Curr Biol* 14 (11), 965-974 (2004).

2 Shibutani, S.T. *et al.*, Intrinsic negative cell cycle regulation provided by PIP box- and Cul4Cdt2-mediated destruction of E2f1 during S phase. *Dev Cell* 15 (6), 890-900 (2008).

3 Lane, M.E. *et al.*, Dacapo, a cyclin-dependent kinase inhibitor, stops cell proliferation during *Drosophila* development. *Cell* 87, 1225-1235 (1996).

4 Keck, J.M. *et al.*, Cyclin E overexpression impairs progression through mitosis by inhibiting APC(Cdh1). *J Cell Biol* 178 (3), 371-385 (2007).

5 Reber, A., Lehner, C.F., & Jacobs, H.W., Terminal mitoses require negative regulation of Fzr/Cdh1 by Cyclin A, preventing premature degradation of mitotic cyclins and String/Cdc25. *Development* 133 (16), 3201-3211 (2006).

6 Sigrist, S.J. & Lehner, C.F., Drosophila fizzy-related down-regulates mitotic cyclins and is required for cell proliferation arrest and entry into endocycles. *Cell* 90 (4), 671-681 (1997).

7 von Dassow, G., Meir, E., Munro, E.M., & Odell, G.M., The segment polarity network is a robust developmental module. *Nature* 406 (6792), 188-192 (2000).

8 Von Dassow, G. & Odell, G.M., Design and constraints of the Drosophila segment polarity module: robust spatial patterning emerges from intertwined cell state switches. *J Exp Zool* 294 (3), 179-215 (2002).

9 Meir, E., von Dassow, G., Munro, E., & Odell, G.M., Robustness, flexibility, and the role of lateral inhibition in the neurogenic network. *Curr Biol* 12 (10), 778-786 (2002).

10 Kim, K.J., Ingeneue: A software tool to simulate and explore genetic regulatory networks in *Systems Biology*, edited by I. V. Maly (Humana Press, New York, 2009), Vol. 500.

11 Meir, E., Munro, E.M., Odell, G.M., & Von Dassow, G., Ingeneue: a versatile tool for reconstituting genetic networks, with examples from the segment polarity network. *J Exp Zool* 294 (3), 216-251 (2002).

12 Kim, K.J. & Fernandes, V.M., Effects of ploidy and recombination on evolution of robustness in a model of the segment polarity network. *PLoS Computational Biology* (in press).

13 MacDonald, N., *Biological Delay Systems: linear stability theory*, 1 ed. (Cambridge University Press, New York, 1989).

[14] Thummel, C.S., Burtis, K.C., & Hogness, D.S., Spatial and temporal patterns of E74 transcription during Drosophila development. *Cell* 61 (1), 101-111 (1990).
[15] Wegrzyn, R.D. & Deuerling, E., Molecular guardians for newborn proteins: ribosome-associated chaperones and their role in protein folding. *Cell Mol Life Sci* 62 (23), 2727-2738 (2005).
[16] Lilly, M.A. & Spradling, A.C., The Drosophila endocycle is controlled by Cyclin E and lacks a checkpoint ensuring S-phase completion. *Genes & Development* 10 (19), 2514-2526 (1996).
[17] Forrester, J.W., *Industrial Dynamics*. (Productivity Press, Cambridge, 1961).
[18] Shcherbata, H.R., Althauser, C., Findley, S.D., & Ruohola-Baker, H., The mitotic-to-endocycle switch in Drosophila follicle cells is executed by Notch-dependent regulation of G1/S, G2/M and M/G1 cell-cycle transitions. *Development* 131 (13), 3169-3181 (2004).
[19] Welcker, M. *et al.*, Multisite phosphorylation by Cdk2 and GSK3 controls cyclin E degradation. *Mol Cell* 12 (2), 381-392 (2003).
[20] Zielke, N., Querings, S., Rottig, C., Lehner, C., & Sprenger, F., The anaphase-promoting complex/cyclosome (APC/C) is required for rereplication control in endoreplication cycles. *Genes Dev* 22 (12), 1690-1703 (2008).
[21] Daga, R.R. & Jimenez, J., Translational control of the cdc25 cell cycle phosphatase: a molecular mechanism coupling mitosis to cell growth. *Journal of Cell Science* 112 Pt 18, 3137-3146 (1999).
[22] Polymenis, M. & Schmidt, E.V., Coupling of cell division to cell growth by translational control of the G_1 cyclin CLN3 in yeast. *Genes and Development* 11, 2522-2531 (1997).
[23] Flybase, http://flybase.bio.indiana.edu/genes/lk/function/.
[24] Weng, L., Zhu, C., Xu, J., & Du, W., Critical role of active repression by E2F and Rb proteins in endoreplication during Drosophila development. *Embo J* 22 (15), 3865-3875 (2003).